iScience

CellPress
OPEN ACCESS

Article

Modeling calcium and magnesium balance: Regulation by calciotropic hormones and adaptations under varying dietary intake

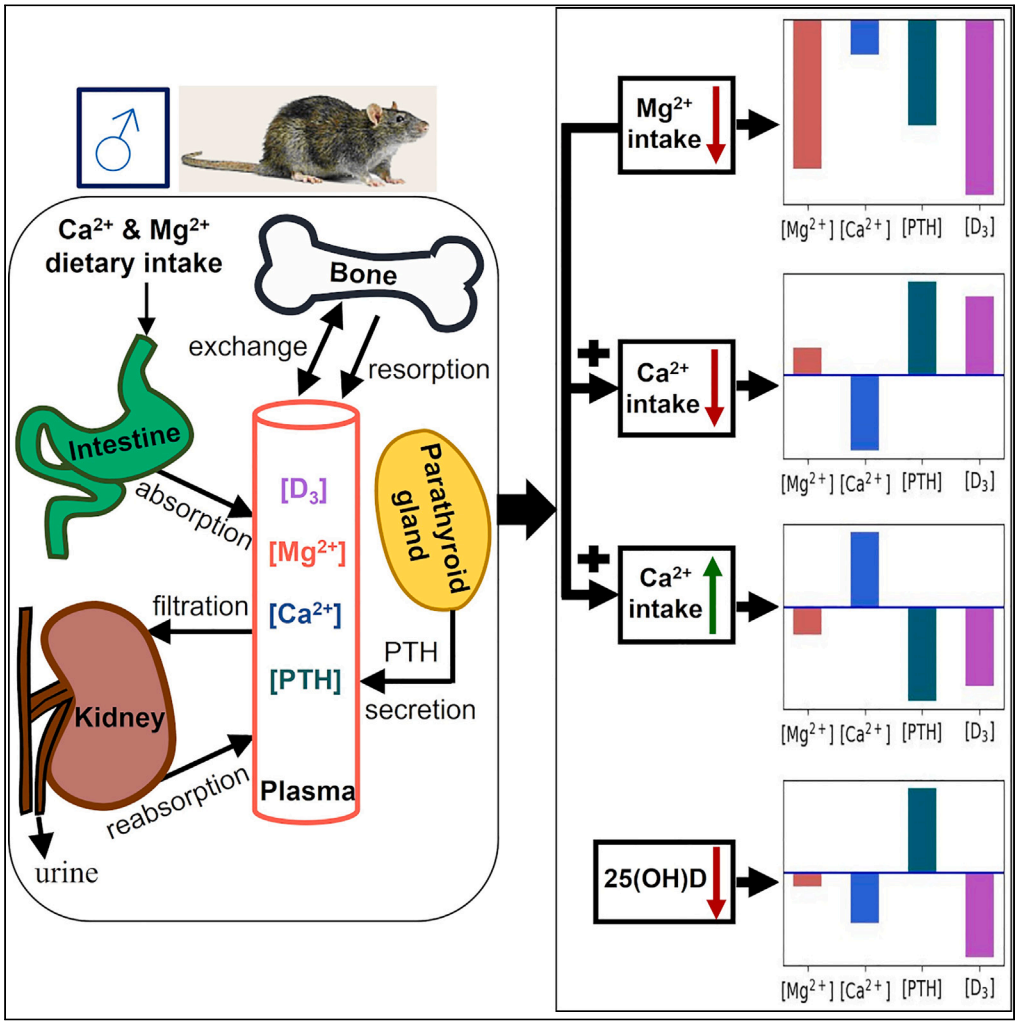

Pritha Dutta, Anita T. Layton

p7dutta@uwaterloo.ca

Highlights

We have developed a computational model of Mg^{2+} and Ca^{2+} homeostasis in a male rat

Severe dietary Mg^{2+} deficiency caused severe hypomagnesemia and mild hypocalcemia

Dietary Ca^{2+} deficiency in the presence of Mg^{2+} deficiency improved plasma Mg^{2+} level

Vitamin D3 deficiency significantly impacted Ca^{2+} homeostasis but not Mg^{2+} homeostasis

Dutta & Layton, iScience 27, 111077
November 15, 2024
https://doi.org/10.1016/j.isci.2024.111077

iScience

CellPress
OPEN ACCESS

Article

Modeling calcium and magnesium balance: Regulation by calciotropic hormones and adaptations under varying dietary intake

Pritha Dutta[1,5,*] and Anita T. Layton[1,2,3,4]

SUMMARY

Magnesium (Mg^{2+}) is crucial for several cellular and physiological processes and is tightly regulated due to health risks associated with imbalances. Mg^{2+}, calcium (Ca^{2+}), parathyroid hormone, and vitamin D_3 are tightly coupled, ensuring proper bone metabolism and intestinal and renal absorption of Mg^{2+} and Ca^{2+}. While several Ca^{2+} homeostasis models exist, no computational model has been developed to study Mg^{2+} homeostasis. We developed a computational model of Mg^{2+} homeostasis in male rats, integrating it with an existing Ca^{2+} homeostasis model, to understand the interconnected physiological processes regulating their homeostasis. We then analyzed adaptations in these interconnected processes under (1) dietary Mg^{2+} deficiency, (2) low/high dietary Ca^{2+} with Mg^{2+} deficiency, and (3) vitamin D_3 deficiency. Model simulations predicted severe hypomagnesemia and mild hypocalcemia with significant dietary Mg^{2+} deficiency. Low dietary Ca^{2+} improved, while high dietary Ca^{2+} worsened Mg^{2+} deficiency. Finally, vitamin D_3 deficiency caused severe hypocalcemia, with minimal impact on Mg^{2+} homeostasis.

INTRODUCTION

Magnesium (Mg^{2+}) is the fourth most abundant cation in the body. Mg^{2+} is the cofactor for several enzymes and hence plays an important role in most major cellular processes such as energy metabolism, DNA transcription, and protein synthesis. In addition, Mg^{2+} is required for muscle contraction, neuromuscular stability, and bone formation. Thus, any disturbance in Mg^{2+} homeostasis can disrupt several essential cellular and physiological processes.

Extracellular Mg^{2+} is tightly regulated, with plasma [Mg^{2+}] maintained relatively constant between 1.6 and 2.3 mg/dL[1] under normal physiological conditions in humans. Mg^{2+} homeostasis is maintained by three organs: the intestine, responsible for Mg^{2+} uptake from diet; bones, responsible for Mg^{2+} storage; and the kidneys, responsible for Mg^{2+} excretion. Almost all of the body's Mg^{2+} (approximately 99%) is either stored in bone or within cells and less than 1% is present in the blood.[1] The normal daily Mg^{2+} intake of humans averages around 300 mg, about half of which is absorbed by the intestine.[2] About 70% of the circulating Mg^{2+} is non-protein-bound and is thus filtered by the glomerulus, accounting for 2,400 mg in humans.

A complex interconnection exists between parathyroid hormone (PTH), calcitriol ($1,25(OH)_2D_3$), Mg^{2+}, and calcium (Ca^{2+}). Mg^{2+} is an important regulator of PTH secretion and vitamin D3 metabolism. Although Mg^{2+} has only ~60% of the effect of Ca^{2+} on PTH secretion, it is still an important regulator of PTH secretion. In fact, acute elevations and reductions in plasma [Mg^{2+}] inhibit PTH secretion irrespective of plasma Ca^{2+} levels. Mg^{2+} also plays an important role in the activation of vitamin D_3 which occurs in two steps: (1) in the liver, cholecalciferol is hydroxylated to 25(OH)D, and (2) in the kidneys, 25(OH)D is converted to $1,25(OH)_2D_3$. The activity of the enzymes involved in both these processes is dependent on Mg^{2+}. Thus, dysregulation of Mg^{2+} homeostasis can significantly impact PTH secretion and vitamin D_3 metabolism which in turn can disrupt bone and Ca^{2+} homeostasis.

Maintaining Mg^{2+} and Ca^{2+} balance relies on the highly coupled regulation of various processes, including intestinal absorption, renal filtration and reabsorption, and bone remodeling. Given the multitude of interconnected physiological processes involved in the homeostasis of these two divalent cations, mathematical modeling proves valuable in comprehending the system's complexities. In this study, we developed the first Mg^{2+} homeostasis model for male rats and integrated it with a previously developed calcium homeostasis model for male rats.[3,4] Figure 1 provides a schematic representation of the fundamental fluxes and hormones involved in Mg^{2+} and Ca^{2+} homeostasis. We then used this model to understand how these different interconnected processes adapt in the presence of different disorders (dietary

[1]Department of Applied Mathematics, University of Waterloo, Waterloo, ON N2L 3G1, Canada
[2]Department of Biology, University of Waterloo, Waterloo, ON N2L 3G1, Canada
[3]Cheriton School of Computer Science, University of Waterloo, Waterloo, ON N2L 3G1, Canada
[4]School of Pharmacology, University of Waterloo, Waterloo, ON N2L 3G1, Canada
[5]Lead contact
*Correspondence: p7dutta@uwaterloo.ca
https://doi.org/10.1016/j.isci.2024.111077

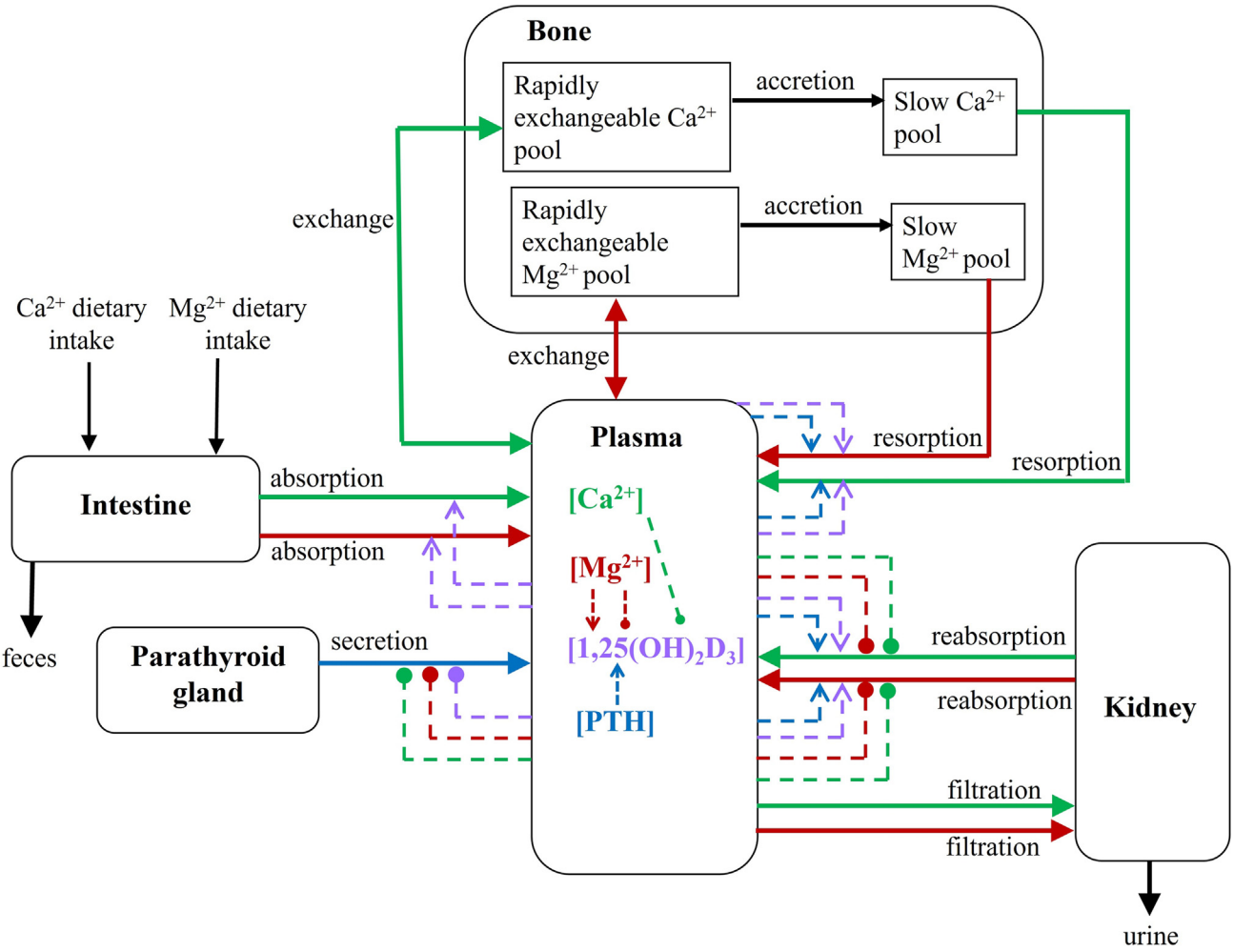

Figure 1. Schematics of the Mg^{2+} homeostasis model

The model consists of five compartments: plasma, intestine, kidney, parathyroid gland, and bone. Arrows with triangular arrowheads indicate activation, while those with circular arrowheads indicate inhibition. All arrows are color coded. Green arrow, Ca^{2+}; red arrow, Mg^{2+}, blue arrow, parathyroid hormone (PTH); mauve arrow, $1,25(OH)_2D_3$.

Mg^{2+} deficiency, low/high dietary Ca^{2+} in the presence of Mg^{2+} deficiency, and vitamin D_3 deficiency) to maintain Mg^{2+} and Ca^{2+} homeostasis.

RESULTS

Baseline results

The predicted baseline steady state concentrations of PTH, $1,25(OH)_2D_3$, Mg^{2+}, and Ca^{2+}, and the steady state Mg^{2+} and Ca^{2+} fluxes are given in Table 1. The predicted baseline $[PTH]_p$, $[1,25(OH)_2D_3]_p$, $[Mg^{2+}]_p$, and $[Ca^{2+}]_p$ fall within the physiological ranges reported in the literature.

Sensitivity analysis

Local sensitivity analysis

We performed a local sensitivity analysis by varying each model parameter listed in Table 2 by $\pm 5\%$ and computing the corresponding steady state. The resulting percent changes in $[PTH]_p$, $[1,25(OH)_2D_3]_p$, $[Mg^{2+}]_p$, and $[Ca^{2+}]_p$ are shown in Figure 4.

A 5% change in minimal thick ascending limb fractional reabsorption λ^0_{Mg-TAL} causes a significant change in $[PTH]_p$, $[1,25(OH)_2D_3]_p$, $[Mg^{2+}]_p$, and $[Ca^{2+}]_p$. Let us analyze the results when λ^0_{Mg-TAL} is increased by 5% (Figure 4A). As intestinal Mg^{2+} absorption is mostly dependent on dietary Mg^{2+} intake and only a small fraction (12%) is regulated by $1,25(OH)_2D_3$ (Equation 19), the kidneys play a major role in determining and maintaining $[Mg^{2+}]_p$. The thick ascending limb is the major Mg^{2+} reabsorption segment in the kidney; hence, a 5% increase in

Table 1. Baseline steady state concentrations and fluxes

	Steady-state value	Range	Source
$[PTH]_p$, pM	6.28	1.5–13	Table 4 of ref.[3] (mathematical model of Ca^{2+} homeostasis in rats),[5,6] (experimental studies on Sprague-Dawley rats)
$[1,25(OH)_2D_3]_p$, pM	154	80–250	Table 4 of ref.[3,7,8] (experimental studies on Sherman rats and Sprague-Dawley rats)
$[Mg^{2+}]_p$, mM	0.65	0.45–0.85	[9–11] (experimental studies on Sprague-Dawley rats and Wistar rats)
$[Ca^{2+}]_p$, mM	1.25	1.1–1.3	Table 4 of ref.[3,5,12] (experimental studies on Sprague-Dawley rats and Wistar Hannover rats)
Intestinal Ca^{2+} absorption, μmol/min	0.59	0.55–1.22	Table 4 of ref.[3]
Intestinal Mg^{2+} absorption, μmol/min	0.032	0.027–0.05	[13] (experimental study on Wistar rats)
Urinary Ca^{2+} excretion, μmol/min	0.045	0.015–0.054	Table 4 of ref.[3]
Urinary Mg^{2+} excretion, μmol/min	0.024	0.01–0.038	[13] (experimental study on Wistar rats)
Bone Ca^{2+} accretion, μmol/min	1.08	–	–
Bone Mg^{2+} accretion, μmol/min	0.02	–	–
Bone Ca^{2+} resorption, μmol/min	0.53	–	–
Bone Mg^{2+} resorption, μmol/min	0.014	–	–
Ca^{2+} flux from fast bone pool to plasma, μmol/min	0.45	–	–
Mg^{2+} flux from fast bone pool to plasma, μmol/min	0.16	–	–
Ca^{2+} flux from plasma to fast bone pool, μmol/min	1.53	–	–
Mg^{2+} flux from plasma to fast bone pool, μmol/min	0.18	–	–

λ^0_{Mg-TAL} increases $[Mg^{2+}]_p$ by 6.7% to 0.69 mM from the baseline value of 0.65 mM (Figure 4). The higher $[Mg^{2+}]_p$ increases the synthesis of $1,25(OH)_2D_3$, which in turn increases the intestinal absorption of Ca^{2+} as 45% of it is regulated by $1,25(OH)_2D_3$.[3] Thus, $[Ca^{2+}]_p$ increases to 1.28 mM from the baseline value of 1.25 mM. $[PTH]_p$ decreases by 5.2% because (1) the increased $[1,25(OH)_2D_3]_p$ inhibits PTH synthesis in the parathyroid gland and (2) the increased $[Mg^{2+}]_p$ and $[Ca^{2+}]_p$ inhibits PTH secretion.

It is interesting to note that the fractional reabsorption of Ca^{2+} along the proximal tubule, which is the major segment of renal Ca^{2+} reabsorption (represented by the parameter λ^0_{Ca-PT}), does not significantly alter $[PTH]_p$, $[1,25(OH)_2D_3]_p$, $[Mg^{2+}]_p$, and $[Ca^{2+}]_p$ (Figure 4). This somewhat unintuitive result is mainly due to the negative feedback loop between $[Ca^{2+}]_p$ and $1,25(OH)_2D_3$ synthesis and PTH secretion. The increased renal Ca^{2+} reabsorption increases $[Ca^{2+}]_p$. This in turn inhibits PTH secretion. The increased $[Ca^{2+}]_p$ and decreased $[PTH]_p$ inhibit $1,25(OH)_2D_3$ synthesis, which in turn inhibits intestinal Ca^{2+} absorption. Thus, the negative feedback loop between $[Ca^{2+}]_p$ and $[1,25(OH)_2D_3]_p$ attenuates the effect on $[Ca^{2+}]_p$ when renal Ca^{2+} reabsorption is varied. By contrast, the feedback loop between $[Mg^{2+}]_p$ and $[1,25(OH)_2D_3]_p$ is reinforcing which contributes to significantly alter $[Mg^{2+}]_p$ in the face of increased/decreased renal Mg^{2+} reabsorption.

Global sensitivity analysis

We conducted global sensitivity analysis by applying the variance-based Sobol method.[20] This method decomposes the output variance into contributions from individual parameters and their interactions, thus identifying parameters that have the most significant effect on the output. Sobol indices are of different orders that reflect the number of parameters interacting with each other. Therefore, the 1st-order Sobol indices measure the effect of individual parameters, 2nd-order Sobol indices measure the effect of the interaction between two parameters and so on. The total Sobol index measures the influence of a parameter, including interactions with other parameters.

We performed the Sobol sensitivity analysis with 10,000 samples. Each parameter listed in Table 2 was varied in the range of ±20%. Figure 5 shows the Sobol indices of parameters that have significant influence on $[PTH]_p$, $[1,25(OH)_2D_3]_p$, $[Mg^{2+}]_p$, and $[Ca^{2+}]_p$. The figure shows the 1st-order Sobol indices (blue bars) and the other order Sobol indices indicating interactions (red bars). The other order index was calculated as total Sobol index − 1st-order Sobol index. The figure shows only those parameters which had total Sobol indices greater than 0.05. For all the parameters, we observe that the 1st-order Sobol indices predominate over the Sobol indices due to interactions. Thus, these parameters individually make significant contributions to the model outputs. Plasma volume (V_p) has the highest influence on $[PTH]_p$, minimal

Table 2. Description and values of model parameters

Parameter	Symbol	Value	Reference
Plasma volume	V_p	10 mL	Granjon et al. [3]
PTH			
Maximal rate constant of PTH secretion from the parathyroid gland	β_{exo}^{PTHg}	1.034 min^{-1}	estimated (refer to section: STAR Methods: Method details: Parathyroid gland and parathyroid hormone and Figure 2)
Factor controlling the maximal PTH secretion at a given plasma Ca^{2+} concentration	γ_{Ca}	0.15 mM	estimated (refer to section: STAR Methods: Method details: Parathyroid gland and parathyroid hormone and Figure 2)
Factor controlling the maximal PTH secretion at a given plasma Ca^{2+} concentration	γ_P	2	estimated (refer to section: STAR Methods: Method details: Parathyroid gland and parathyroid hormone and Figure 2)
Factor controlling the slope of the PTH secretion curve	C_m	3.8 mM	estimated (refer to section: STAR Methods: Method details: Parathyroid gland and parathyroid hormone and Figure 2)
IC_{50} value of Mg^{2+} for inhibition of PTH secretion	K_{low-Mg}	0.25 mM	Quitterer et al. [14]
Basal rate of PTH production in the parathyroid gland	k_{prod}^{PTHg}	2.53 pmol/min	estimated
Inhibition of PTH synthesis by $1,25(OH)_2D_3$	$\gamma_{prod}^{1,25(OH)_2D_3}$	0.003 $p.m.^{-1}$	Stadt et al.[4]
Rate of degradation of PTH in parathyroid gland	k_{deg}^{PTHg}	0.035 min^{-1}	Granjon et al. [3]
Degradation rate constant of plasma PTH	k_{deg}^{PTHp}	0.081 min^{-1}	estimated
Vitamin D_3			
Inactive vitamin D_3	$[25(OH)D]_p$	25 nM	Granjon et al. [3]
Minimum production rate constant of $1,25(OH)_2D_3$	k_{conv}^{min}	4.4×10^{-6} min^{-1}	Granjon et al. [3]
Maximal increase in $1,25(OH)_2D_3$ production rate	δ_{conv}^{max}	6×10^{-5} min^{-1}	Granjon et al. [3]
Stimulation of $1,25(OH)_2D_3$ production by PTH	K_{conv}^{PTH}	3 p.m.	Granjon et al. [3]
PTH sensitivity coefficient	n_{conv}	6	Granjon et al. [3]
Inhibition of $1,25(OH)_2D_3$ production by Ca^{2+}	γ_{conv}^{Ca}	0.3 mM^{-1}	Granjon et al. [3]
Inhibition of $1,25(OH)_2D_3$ production by itself	$\gamma_{conv}^{1,25(OH)_2D_3}$	1.8×10^{-2} $p.m.^{-1}$	Granjon et al. [3]
Factor controlling the maximal increase in $1,25(OH)_2D_3$ production by Mg^{2+}	δ_{Mg-act}	6.6	estimated (refer to section: STAR Methods: Method details: Plasma $1,25(OH)_2D_3$ and Figure 3)
Michaelis-Menten constant	K_{Mg-act}^1	1.1 mM	estimated (refer to section: STAR Methods: Method details: Plasma $1,25(OH)_2D_3$ and Figure 3)
Michaelis-Menten constant	K_{Mg-act}^2	1.2 mM	estimated (refer to section: STAR Methods: Method details: Plasma $1,25(OH)_2D_3$ and Figure 3)
Inhibition of $1,25(OH)_2D_3$ degradation by PTH	γ_{inact}^{PTH}	0.52 $p.m.^{-1}$	Granjon et al. [3]
Michaelis-Menten constant	K_{D3}	1.7 mM	estimated
Degradation rate constant of $1,25(OH)_2D_3$	$k_{deg}^{1,25(OH)_2D_3}$	0.008 min^{-1}	estimated
Kidneys			
Minimal fractional reabsorption of Mg^{2+} in proximal tubule	λ_{Mg-PT}^0	0.185	Quamme et al.[15]

(*Continued on next page*)

Table 2. *Continued*

Parameter	Symbol	Value	Reference
Stimulation of Mg^{2+} reabsorption in proximal tubule by PTH	δ^{max}_{Mg-PT}	0.015	estimated
Sensitivity of Mg^{2+} reabsorption in proximal tubule to PTH	PTH_{ref}	12 p.m.	Granjon et al. [3]
Hill coefficient	n_{PT}	5	Granjon et al. [3]
Minimal fractional reabsorption of Mg^{2+} in thick ascending limb	λ^{0}_{Mg-TAL}	0.66	Quamme et al.[15]
Stimulation of Mg^{2+} reabsorption in thick ascending limb by CaSR	$\delta^{max}_{Mg-CaSR}$	0.028	estimated
Stimulation of Mg^{2+} reabsorption in thick ascending limb by PTH	δ^{max}_{Mg-PTH}	0.012	estimated
Sensitivity of Mg^{2+} reabsorption in thick ascending limb to Ca^{2+}	Ca_{ref}	1.25 mM	Brown et al. [16]
Sensitivity of Mg^{2+} reabsorption in thick ascending limb to Mg^{2+}	Mg_{ref}	2.5 mM	Brown et al. [16]
Hill coefficient	n_{TAL}	4	Granjon et al. [3]
Sensitivity of Mg^{2+} reabsorption in thick ascending limb to PTH	K^{PTH}_{TAL}	4 p.m.	Stadt et al.[4]
Minimal fractional reabsorption of Mg^{2+} in distal convoluted tubule	λ^{0}_{Mg-DCT}	0.08	Quamme et al.[15]
Stimulation of Mg^{2+} reabsorption in distal convoluted tubule by PTH and $1,25(OH)_2D_3$	δ^{max}_{Mg-DCT}	0.02	estimated
Sensitivity of Mg^{2+} reabsorption in distal convoluted tubule to PTH	K^{PTH}_{DCT}	7.25 p.m.	Stadt et al. [4]
Sensitivity of Mg^{2+} reabsorption in distal convoluted tubule to $1,25(OH)_2D_3$	$K^{1,25(OH)_2D_3}_{DCT}$	160 p.m.	Stadt et al. [4]
Glomerular filtration rate (GFR)	Φ_{GFR}	1.25 mL/min	Sadick et al. [17]
Intestine			
Dietary Mg^{2+} intake	I_{Mg}	0.04 μmol/min	Coudray et al. [13]
Maximal rate of active absorption of Mg^{2+}	V_{active}	0.764 μmol/min	Hardwick et al.[18]
Stimulation of active Mg^{2+} absorption by dietary Mg^{2+} intake	K_{active}	0.17 μmol/min	Hardwick et al.[18]
Stimulation of Mg^{2+} absorption by $1,25(OH)_2D_3$	$K^{1,25(OH)_2D_3}_{abs}$	100 p.m.	Granjon et al. [3]
Bones			
Rate of Mg^{2+} uptake from plasma by fast bone pool	k^{Mg}_{p-f}	0.074 min^{-1}	estimated
Rate of Mg^{2+} release from fast bone pool to plasma	k^{Mg}_{f-p}	0.2 x 10^{-3} min^{-1}	estimated
Rate of accretion into the slow bone pool	γ^{Mg}_{ac}	3.98 x 10^{-4} min^{-1}	estimated
Minimal resorption rate	τ^{min}_{res}	0.142 x 10^{-3} mmol/min	Granjon et al. [3]
Maximal resorption rate	δ^{max}_{res}	0.7 x 10^{-3} mmol/min	Granjon et al. [3]
Stimulation of bone resorption by PTH	K^{PTHp}_{res}	2.45 p.m.	Granjon et al. [3]
Stimulation of bone resorption by $1,25(OH)_2D_3$	$K^{1,25(OH)_2D_3}_{res}$	160 p.m.	Granjon et al. [3]
Plasma			
Fraction of magnesium bound to proteins	κ_{b-Mg}	0.3	Jahnen-Dechent et al. [19]

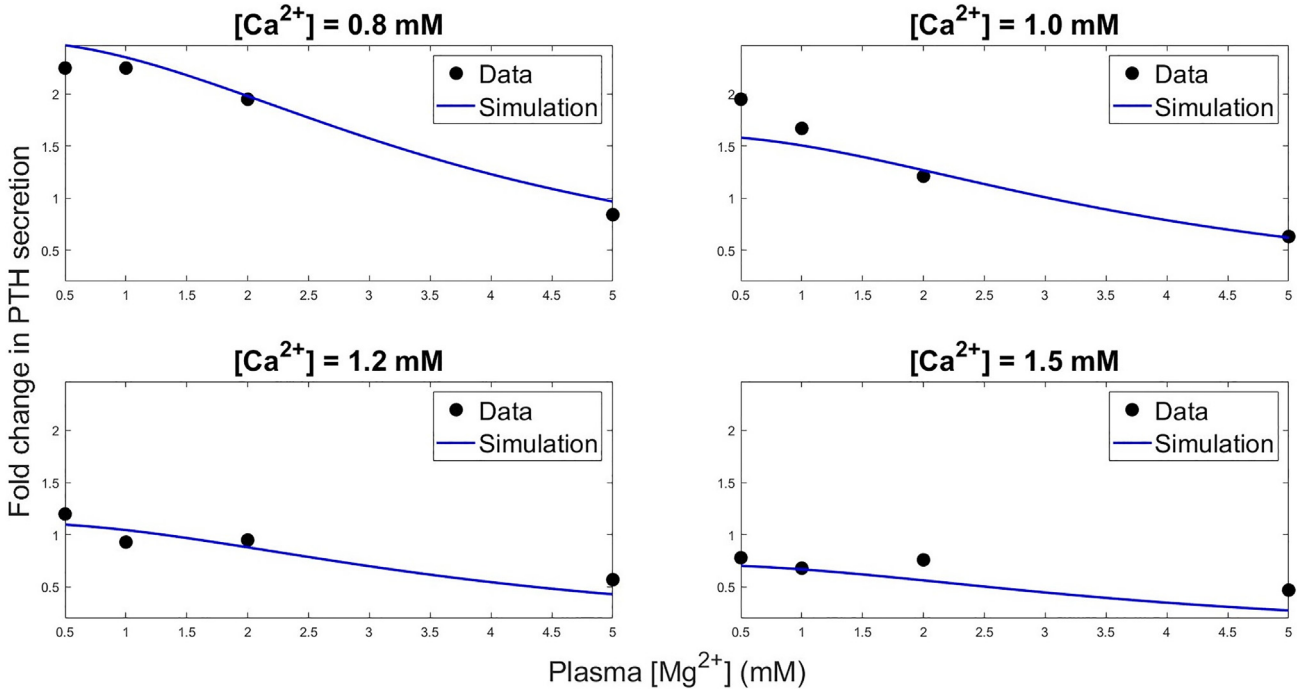

Figure 2. Comparison between experimental and simulated changes in PTH secretion at different plasma Ca^{2+} and Mg^{2+} concentrations

The lsqcurvefit function of MATLAB, which is a non-linear least-square solver, was used to fit our model simulations to experimental values.

fractional reabsorption of Mg^{2+} in thick ascending limb (λ^0_{Mg-TAL}) has the most impact on $[1,25(OH)_2D_3]_p$ and $[Mg^{2+}]_p$, and rate of Ca^{2+} uptake from plasma by fast bone pool (k^{Ca}_{pf}) has the highest impact on $[Ca^{2+}]_p$.

Effect of deficiency of dietary Mg^{2+}

A large portion of the population in all continents consumes less than two-thirds of the recommended dietary allowances for Mg^{2+}.[21] In the United States, the standard diet contains only about 50% of the recommended daily Mg^{2+}.[22] Insufficient dietary Mg^{2+} intake may lower plasma Mg^{2+} level which can have severe consequences. For instance, vitamin D metabolizing enzymes, 1α-hydroxylase and 24-hydroxylase, are Mg^{2+}-dependent and hence Mg^{2+} deficiency can significantly lower plasma $1,25(OH)_2D_3$ levels.[23,24] In addition, Mg^{2+} deficiency also impairs PTH response. To evaluate its effect on Ca^{2+} and Mg^{2+} homeostasis, we conducted simulations in which dietary Mg^{2+} intake (I_{Mg}) was reduced by 50%, 75%, and 90% for 6 months according to the experiments conducted by Rude et al.[9,25,26] The predicted fractional changes in plasma concentrations of PTH, $1,25(OH)_2D_3$, Mg^{2+}, and Ca^{2+} and Mg^{2+} and Ca^{2+} fluxes after 6 months of restricted I_{Mg} are shown in Figure 6.

Figure 6A shows the predicted and experimental[9,25,26] fractional changes in $[PTH]_p$, $[1,25(OH)_2D_3]_p$, $[Mg^{2+}]_p$, $[Ca^{2+}]_p$, bone Ca^{2+} content, and bone Mg^{2+} content at different I_{Mg} restrictions. Bone Ca^{2+} and Mg^{2+} contents were measured from bone ash in the experimental studies.[9,25,26] The predicted fractional changes in $[PTH]_p$, $[1,25(OH)_2D_3]_p$, $[Mg^{2+}]_p$, and bone Mg^{2+} content are almost in line with the experimentally reported changes. However, while the experimental study reported $[Mg^{2+}]_p$ to decrease by 6% at 50% I_{Mg} restriction, the model predicted a decrease of 17%. The model might have underestimated the adaptive increase in intestinal Mg^{2+} absorption at moderate Mg^{2+} deficiency in rats, since the intestinal absorption parameters were obtained from a study conducted on humans. Nevertheless, the predicted $[Mg^{2+}]_p$ at 50% I_{Mg} restriction (0.54 mM) is within the normal range (0.45–0.85 mM). In addition, the predicted change in $[Ca^{2+}]_p$ content differs significantly from the experimental values. The experimental studies[9,25,26] reported $[Ca^{2+}]_p$ to decrease by 5% at 50% I_{Mg} restriction, and increase by 5% and 9% at 75% and 90% I_{Mg} restrictions, respectively. By contrast, our model predicted $[Ca^{2+}]_p$ to decrease by 10%, 20%, and 23% after 6 months of 50%, 75%, and 90% I_{Mg} restrictions, respectively. Severe dietary Mg^{2+} deficiency causes hypocalcemia in most species (including humans[27,28]) with the exception of rats and mice, where hypercalcemia develops.[29] The exact reasons for this are not clearly understood but could be due to the reduction in osteoblastic and osteocytic activity in the presence of hypomagnesemia, which significantly lowers the rate of bone formation.[29–31] Further investigation is required to understand why severe dietary Mg^{2+} deficiency results in hypercalcemia in rodents and hypocalcemia in other species.

At 50% I_{Mg} restriction, $[Mg^{2+}]_p$ was predicted to decrease to 0.54 mM from the baseline concentration of 0.65 mM, and $[Ca^{2+}]_p$ decreased to 1.12 mM from the baseline concentration of 1.25 mM, thus triggering increased PTH secretion (Figure 6A). By contrast, at 75% and 90% I_{Mg} restrictions, $[Mg^{2+}]_p$ was predicted to decrease to 0.31 and 0.17 mM, respectively, which are significantly below 0.4 mM. These very low plasma

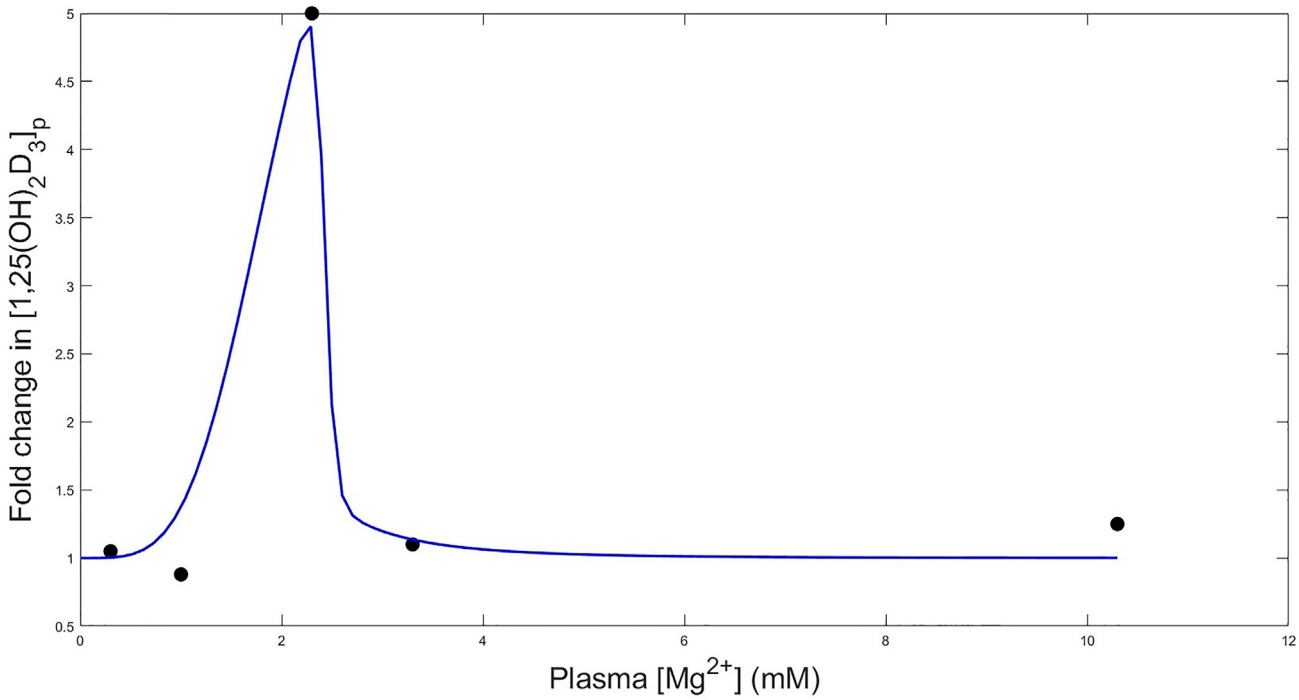

Figure 3. Comparison between experimental and simulated changes in $[1,25(OH)_2D_3]_p$ at different plasma Mg^{2+} concentrations

The lsqcurvefit function of MATLAB was used to fit our model simulations to experimental values.

Mg^{2+} concentrations inhibit PTH secretion (based on Equation 5). Similar observations were reported in dietary Mg^{2+} restriction experiments conducted on humans.[32] Intestinal Mg^{2+} absorption was predicted to decrease proportionally with the I_{Mg} restrictions (Figure 6B). Since 45% of intestinal Ca^{2+} absorption is regulated by $[1,25(OH)_2D_3]_p$, it was predicted to decrease by 13%, 21%, and 22%, respectively (Figure 6B). Urinary Ca^{2+} and Mg^{2+} excretions decreased proportionally with decrease in $[Ca^{2+}]_p$ and $[Mg^{2+}]_p$ (Figure 6C).

Dietary Mg^{2+} reduction causes significant bone loss.[9,25,26,33] Bone loss is characterized by a decrease in bone mineral density (i.e., decrease in Ca^{2+}, Mg^{2+}, and other mineral content in the bone). Our model predicted bone Mg^{2+} content to decrease by 9%, 17%, and 39%, respectively, following 6 months of 50%, 75%, and 90% I_{Mg} restrictions (Figure 6A), which are in line with the experimental values.[9,25,26] Several experimental and clinical studies have shown that Mg^{2+} deficiency promotes osteoporosis (summarized in[34]). Due to this bone loss, the exchange of Mg^{2+} between the bone and plasma drops significantly (Figures 6B and 6C). The model predicted almost no change in bone Ca^{2+}, in line with the experimental results.(Figure 6A).

Taken together, model results reveal the mechanisms by which sufficiently large deficiency in dietary Mg^{2+} causes dysregulation in Ca^{2+} and Mg^{2+} homeostasis.

Effect of low/high dietary Ca^{2+} in the presence of low dietary Mg^{2+}

Since, as noted previously, a large portion of the population consumes Mg^{2+} lower than the recommended level, we investigated the effect that low dietary Ca^{2+} or Ca^{2+} supplementation has on Ca^{2+} and Mg^{2+} homeostasis in the presence of 60% dietary Mg^{2+} (I_{Mg}) restriction. To simulate low and high dietary Ca^{2+}, we decreased and increased I_{Ca} by 50%, respectively. Figure 7 shows the predicted fractional changes in steady state plasma concentrations of PTH, $1,25(OH)_2D_3$, Mg^{2+}, and Ca^{2+} and the steady state Mg^{2+} and Ca^{2+} fluxes from the steady state values at 60% I_{Mg} restriction (shown by the gray line at 0) for each set of simulations.

At 60% I_{Mg} restriction and baseline I_{Ca}, $[Mg^{2+}]_p$ decreased by 31% to 0.45 mM from the baseline concentration of 0.65 mM and $[Ca^{2+}]_p$ decreased by 13% to 1.08 mM from the baseline concentration of 1.25 mM. Restricting I_{Ca} by 50% further lowered $[Ca^{2+}]_p$ to 0.88 mM, resulting in hypocalcemia (Figure 7A). This enhanced PTH secretion (Equation 2). The decreased $[Ca^{2+}]_p$ and increased $[PTH]_p$ enhanced $1,25(OH)_2D_3$ synthesis (Equation 7). The increased $[PTH]_p$ and $[1,25(OH)_2D_3]_p$ increased resorption of Mg^{2+} from the slow bone pool by 13% (Equation 22). In addition, the increased $[1,25(OH)_2D_3]_p$ enhanced intestinal absorption of Mg^{2+} raising $[Mg^{2+}]_p$ to 0.49 mM (Figure 7A). Thus, lowering dietary Ca^{2+} intake during dietary Mg^{2+} deficiency improved plasma Mg^{2+} concentration and ameliorated hypomagnesemia.[35]

The opposite changes were observed when I_{Ca} was increased by 50%. $[Ca^{2+}]_p$ increased to 1.21 mM which inhibited PTH secretion and $1,25(OH)_2D_3$ synthesis (Figure 7A). This in turn inhibited resorption of Mg^{2+} from the slow bone pool and intestinal Mg^{2+} absorption.

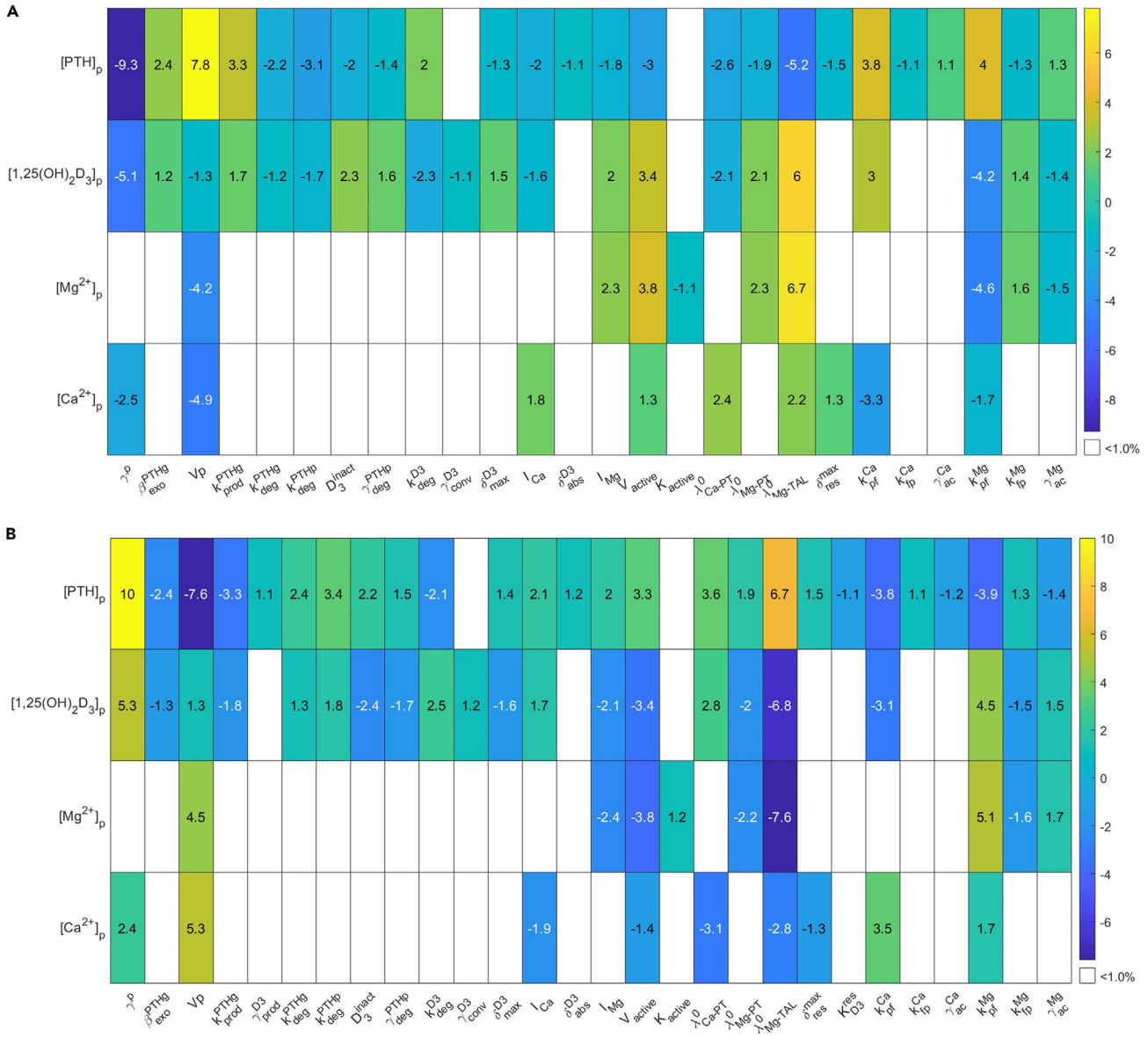

Figure 4. Local sensitivity analysis

Local sensitivity analysis conducted by (A) increasing individual parameters by 5% and (B) decreasing individual parameters by 5%. The resulting percent change in model steady state concentrations from baseline is presented here. White indicates the resulting change was less than 1%.

Consequently, $[Mg^{2+}]_p$ decreased further from 0.45 mM to 0.41 mM (Figure 7A). Thus, higher dietary Ca^{2+} intake combined with dietary Mg^{2+} deficiency exacerbated hypomagnesemia.[36–39]

To understand these changes in the cellular level, note that when I_{Ca} is decreased, $[Ca^{2+}]_p$ decreases, which stimulates the calcium-sensing receptors (CaSR) on the parathyroid glands and PTH secretion increases. Now Ca^{2+} is an inhibitor and PTH is an activator of 1α-hydroxylase, the enzyme responsible for converting 25(OH)D to $1,25(OH)_2D_3$. Thus, the decreased plasma Ca^{2+} and increased plasma PTH increase the synthesis of $1,25(OH)_2D_3$. The increased PTH and $1,25(OH)_2D_3$ increase production of release receptor activator of nuclear factor kappa-B ligand (RANKL) and osteoprotegerin (OPG), leading to increased osteoclast formation and activity and hence increased bone resorption. Along the renal thick ascending limb, increased PTH decreases claudin 14 and activated CaSR increases claudin 14 expression; these two opposing responses slightly increase claudin 16/19 expression and hence paracellular transport of Mg^{2+}. Along the renal distal convoluted tubule, PTH increases Mg^{2+} uptake through receptor-mediated cAMP release and activation of protein kinase A and $1,25(OH)_2D_3$ increases Mg^{2+} uptake through calbindin-D. All these responses combine to increase plasma Mg^{2+} concentration. The opposite responses occur when I_{Ca} is increased. Taken together, reduced dietary Ca^{2+} intake in

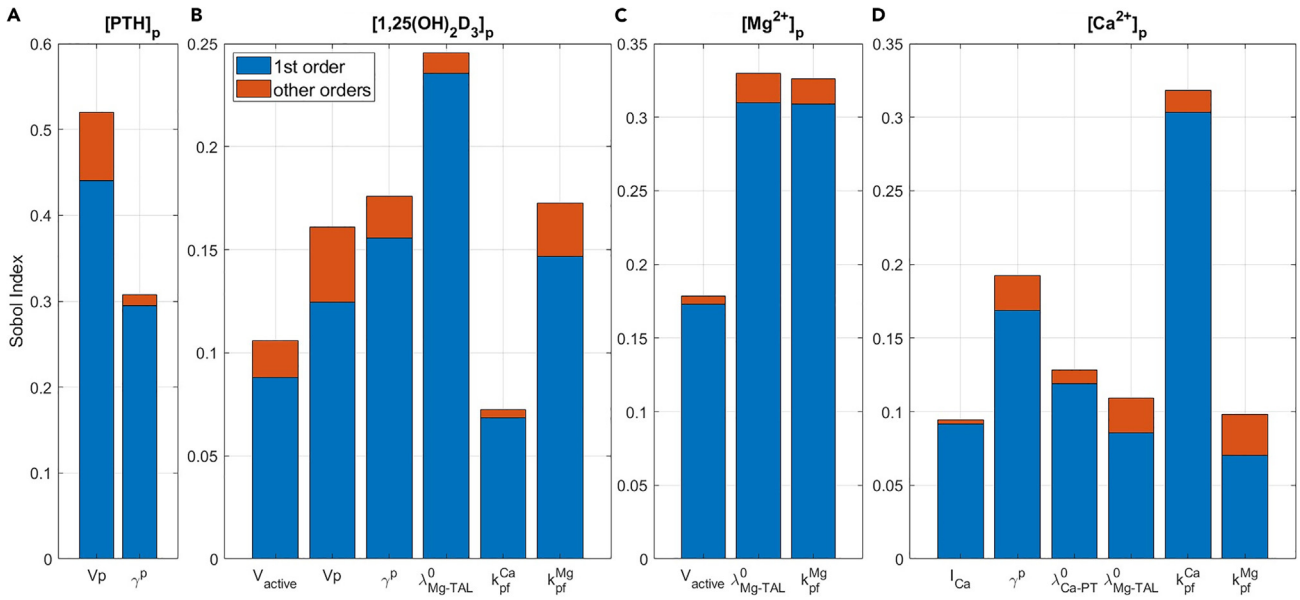

Figure 5. Global sensitivity analysis

Sobol indices of parameters that have significant impact on (A) $[PTH]_p$, (B) $[1,25(OH)_2D_3]_p$, (C) $[Mg^{2+}]_p$, and (D) $[Ca^{2+}]_p$. Parameters were varied in the range of ±20% and Sobol indices were calculated on steady state concentrations.

Parameters with total Sobol indices greater than 0.05 are shown. Blue bars indicate the 1st-order Sobol indices and red bars indicate the other order indices representing interaction with other parameters. The other order indices were calculated as total Sobol indices − 1st-order Sobol indices.

the presence of Mg^{2+} deficiency helped to improve plasma Mg^{2+} concentration, whereas, increased dietary Ca^{2+} intake caused further decline in plasma Mg^{2+} concentration.

Effect of change of inactive vitamin D3 (25(OH)D)

Low plasma level of 25(OH)D, the substrate for $1,25(OH)_2D_3$ (Figure 8), is commonly observed in chronic liver disease and chronic kidney disease, with the degree of 25(OH)D deficiency increasing with the severity and progression of disease.[40–44] Since $1,25(OH)_2D_3$ plays an important role in Mg^{2+} and Ca^{2+} homeostasis, we studied the effect of different levels of 25(OH)D deficiency on Mg^{2+} and Ca^{2+} homeostasis. To accomplish that, we progressively decreased the parameter $[25(OH)D]_p$ up to 100%. The predicted normalized steady state plasma concentrations of PTH, $1,25(OH)_2D_3$, Mg^{2+}, and Ca^{2+} and the normalized steady state Mg^{2+} and Ca^{2+} fluxes are shown in Figure 9.

As $[25(OH)D]_p$ was decreased, $1,25(OH)_2D_3$ synthesis in the kidneys decreased, resulting in lower $[1,25(OH)_2D_3]_p$ (Equation 7), which became zero when $[25(OH)D]_p = 0$ (Figure 9A). Now, $[1,25(OH)_2D_3]_p$ directly and indirectly regulates the following: (1) PTH synthesis, (2) intestinal absorption of Ca^{2+} and Mg^{2+}, (3) renal Ca^{2+} and Mg^{2+} reabsorption, and (4) bone resorption. Let us first assess the impact on intestinal absorption of Mg^{2+} and Ca^{2+}. $[1,25(OH)_2D_3]_p$ regulates 45% of intestinal Ca^{2+} absorption[3] but only 12% of intestinal Mg^{2+} absorption (Equation 19). Hence, the decrease in intestinal Ca^{2+} absorption[45] was significantly higher compared to Mg^{2+} (Figure 9B). Consequently, $[Ca^{2+}]_p$ decreased by 14% to 1.08 mM (below the normal range of 1.1–1.3 mM) at 50% inhibition of $[25(OH)D]_p$, and further by 54% to 0.58 mM, which was significantly below the normal range (Figure 9A), at full inhibition. Several experimental and clinical studies have reported hypocalcemia in the presence of low serum 25(OH)D concentration.[45–47] By contrast, $[Mg^{2+}]_p$ did not change significantly until $[25(OH)D]_p$ was inhibited by over 60%, at which point $[Mg^{2+}]_p$ was about 2.4% lower than baseline (Figure 9A). At full inhibition, $[Mg^{2+}]_p$ dropped by 11% to 0.58 mM, within the normal range (normal range is 0.45–0.85 mM) (Figure 9A). The lower $[Ca^{2+}]_p$ and $[Mg^{2+}]_p$ enhanced PTH secretion to maintain levels of these two divalent cations (Equation 2). In addition, the inhibitory effect of $[1,25(OH)_2D_3]_p$ on PTH synthesis in the parathyroid gland (Equation 1) was attenuated, which further increased PTH secretion. Thus, $[PTH]_p$ increased by 29% and 193%, respectively, at 50% and 100% inhibitions (Figure 9A).[48] Now, the higher $[PTH]_p$ increased Ca^{2+} and Mg^{2+} reabsorption along the thick ascending limb and distal convoluted tubule. In addition, the fall in $[Ca^{2+}]_p$ and $[Mg^{2+}]_p$ also decreased the Ca^{2+} and Mg^{2+} loads filtered by the kidneys. These two factors contributed to reducing urinary excretion of Ca^{2+} and Mg^{2+} to preserve plasma levels of these cations. Ca^{2+} and Mg^{2+} excretions decreased by 13% and 8% respectively, following a 50% inhibition of $[25(OH)D]_p$, and by 26% and 13% respectively, when $[25(OH)D]_p$ was fully inhibited (Figure 9C).

Following the significant decrease in $[Ca^{2+}]_p$, the exchange of Ca^{2+} between bone and plasma decreased significantly (Figures 9B and 9C). The decrease in Mg^{2+} exchange was comparatively lower (Figures 9B and 9C). Ca^{2+} content in the fast bone pool was predicted to decrease by 13% and 47% respectively, whereas the Mg^{2+} content decreased by 1.2% and 8.5%, respectively, at 50% and 100% $[25(OH)D]_p$ inhibition

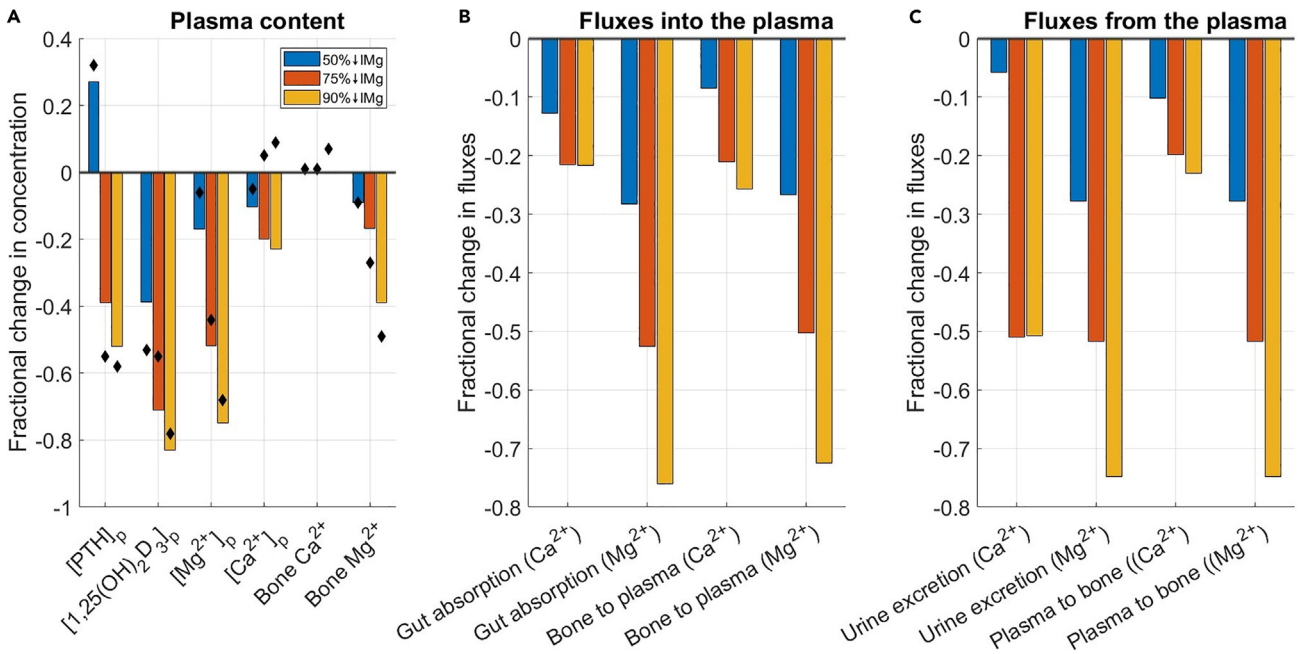

Figure 6. Dietary Mg^{2+} deficiency

Predicted fractional changes in plasma concentrations and fluxes at 50%, 75%, and 90% dietary Mg^{2+} intake (I_{Mg}) restrictions from baseline (denoted by the gray line at 0) for 6 months (A) Predicted (bars) and experimental (black diamonds) fractional changes in plasma concentrations of PTH, $1,25(OH)_2D_3$, Ca^{2+}, Mg^{2+}, bone Ca^{2+} content, and bone Mg^{2+} content.

(B) Predicted fractional changes in Mg^{2+} and Ca^{2+} fluxes into plasma.

(C) Predicted fractional changes in Mg^{2+} and Ca^{2+} fluxes out of plasma.

(Figure 9A). Now in the slow bone pool, Ca^{2+} content decreased by 4.9% and 24% respectively (Figure 9A). By contrast, our model predicted the Mg^{2+} content in the slow bone pool to remain almost unchanged (Figure 9A).

These results indicated that $1,25(OH)_2D_3$ plays a major role in maintaining Ca^{2+} homeostasis as its deficiency can cause severe hypocalcemia.[49] Mg^{2+} homeostasis on the other hand is not severely impacted by deficiency of $1,25(OH)_2D_3$.[49]

Recall that the model predicted that a decrease in plasma Ca^{2+} in response to dietary Ca^{2+} restriction would increase plasma Mg^{2+} level (section: Effect of low/high dietary Ca^{2+} in the presence of low dietary Mg^{2+}). However, a decrease in plasma Ca^{2+} level in response to 25(OH)D inhibition resulted in a decrease in plasma Mg^{2+} level (section: Effect of change of inactive vitamin D3 (25(OH)D)). Why does a decrease in plasma Ca^{2+} level cause opposite changes in plasma Mg^{2+} level in these two scenarios? Figure 10 summarizes the responses in these two scenarios which help answer this question. The difference lies in the change in plasma $1,25(OH)_2D_3$. During dietary Ca^{2+} restriction, plasma $1,25(OH)_2D_3$ increases which together with the increased plasma PTH increase Mg^{2+} reabsorption along the distal convoluted tubule and bone resorption. By contrast, during 25(OH)D inhibition, plasma $1,25(OH)_2D_3$ decreases significantly, which inhibits Mg^{2+} reabsorption along the distal convoluted tubule and bone resorption. Thus, plasma Mg^{2+} increases during dietary Ca^{2+} restriction and decreases during 25(OH)D inhibition.

DISCUSSION

Mg^{2+} balance is primarily maintained by the absorption of Mg^{2+} in the intestine and kidney. Typically, approximately 30–50% of ingested Mg^{2+} is absorbed by the intestine. The refining and processing of food in modern society has resulted in a substantial loss of the naturally occurring Mg^{2+}. For example, the refining and processing of wheat to flour, rice to polished rice, and corn to starch depletes Mg^{2+} by >80%.[50] Thus, the consumption of modern processed food may partially explain why a significant segment of the population has an Mg^{2+} intake that falls below the recommended dietary amounts. The intestine absorbs a fraction of Mg^{2+} that is inversely proportional to intake.[18] This may have an unfortunate clinical consequence of prolonging the time for the treatment of Mg^{2+} deficiency with oral supplements to be effective. In the kidneys, the proximal tubule accounts for 15–25% of Mg^{2+} reabsorption, the thick ascending limb for 60–70%, and the distal convoluted tubule for ~10%.[51] Intestinal and renal Mg^{2+} transport occurs through both paracellular and transcellular pathways. Approximately 90% of Mg^{2+} absorption in the intestine and kidneys occurs passively through the paracellular pathway. Active reabsorption of Mg^{2+} occurs transcellularly. Although it accounts for only a small fraction of the total intestinal and kidney absorption, active Mg^{2+} transport is regulated and therefore fine tunes intestinal and renal Mg^{2+} excretion.

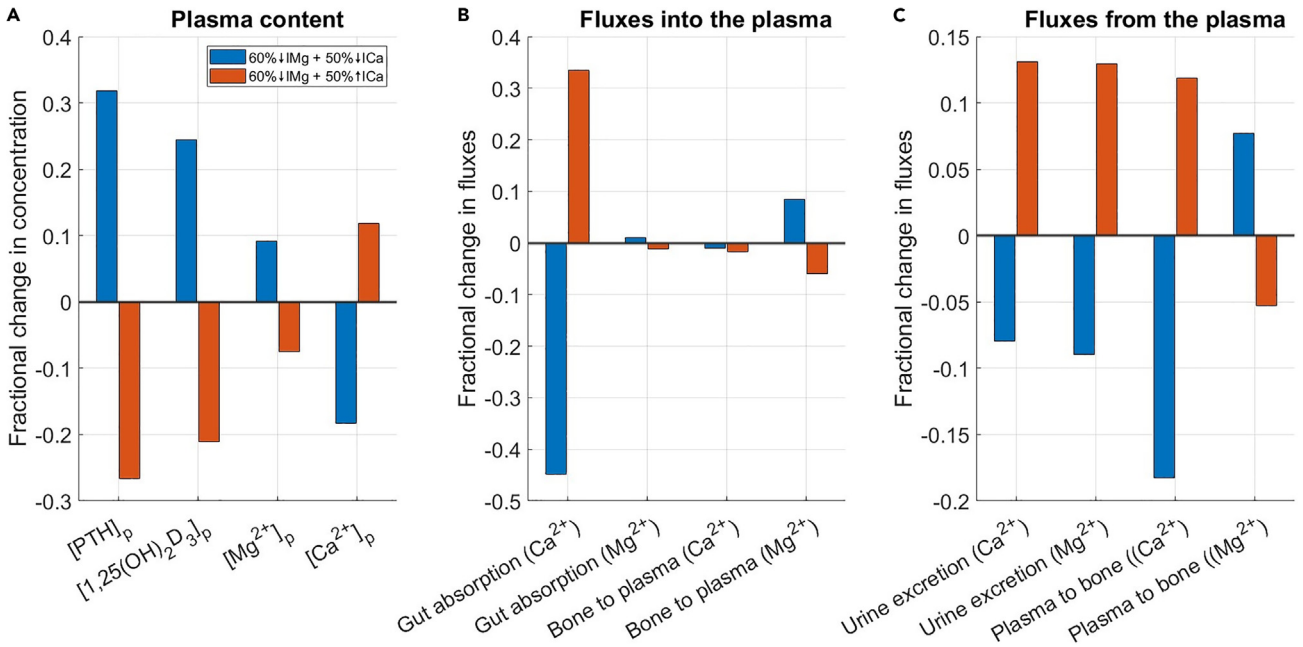

Figure 7. Dietary Ca^{2+} deficiency or supplementation in the presence of dietary Mg^{2+} deficiency

Predicted fractional change in steady state plasma concentrations and fluxes at (i) 60% dietary Mg^{2+} (I_{Mg}) restriction combined with 50% dietary Ca^{2+} (I_{Ca}) restriction and (ii) 60% I_{Mg} restriction combined with 50% I_{Ca} increase from the steady state values at 60% I_{Mg} restriction (shown by the gray line at 0).

(A–C) (A) Fractional change in steady state plasma concentrations of PTH, $1,25(OH)_2D_3$, Ca^{2+}, and Mg^{2+}. (B) Fractional change in steady state Mg^{2+} and Ca^{2+} fluxes into plasma. (C) Fractional change in steady state Mg^{2+} and Ca^{2+} fluxes out of plasma.

Hypomagnesemia is not uncommon, especially among hospitalized patients (up to 12%).[52] Hypomagnesemia can be caused by decreased intake and absorption, or increased losses and redistribution. We considered the physiological implications of low Mg^{2+} intake (model predictions summarized in Figure 11). Model simulations indicated that severe Mg^{2+} deficiency leads to hypocalcemia and bone loss (Figure 6). Indeed, Mg^{2+} deficiency has been implicated as a risk factor for osteoporosis. Epidemiological studies[53–55] have demonstrated a positive correlation between dietary Mg^{2+} intake and bone density and/or an increased rate of bone loss with low dietary Mg^{2+} intake. In mouse studies,[29] Mg^{2+} depletion has also been reported to induce impaired bone growth, decreased osteoblast number, increased osteoclast number, and loss of trabecular bone with stimulation of cytokine activity in bone.

Besides a low Mg^{2+} diet, low Mg^{2+} input can also be caused by decreased absorption. Gastrointestinal diseases that reduce the transit time of intestinal fluid or interfere with absorption can also cause hypomagnesemia. Examples of such gastrointestinal diseases include severe diarrhea, steatorrhea, malabsorption syndromes, and short-bowel syndrome. The capacity of the intestine to absorb dietary Mg^{2+} also declines with aging.[56] As such, aging is a major risk factor for Mg^{2+} deficiency.

The causes of renal Mg^{2+} loss can be further divided into those due to increased flow, for example in case of polyuria, and those due to decreased tubular reabsorption. The causes of decreased tubular reabsorption of Mg^{2+} can, in turn, be classified according to the location in the nephron at which Mg^{2+} transport is perturbed. Because the thick ascending limb and the distal convoluted tubule are the major sites of renal Mg^{2+} reabsorption, most causes affect these regions of the kidney. For instance, Type 1 Bartter's syndrome and Gitelman's syndrome, which inhibit Na^+ transporters along the thick ascending limb and distal convoluted tubule, respectively, cause increased Mg^{2+} excretion.[57,58]

The body's handling of Ca^{2+} and Mg^{2+} is coupled in the kidneys and via their regulation by PTH and vitamin D. Approximately half of the world's population has inadequate access to dietary Ca^{2+}.[59] Inadequate Ca^{2+} intake is linked not only to poor bone health but to other negative health outcomes, including pregnancy complications, cancers, and cardiovascular disease. As such, Ca^{2+} supplementation is often recommended to vulnerable subpopulations such as pregnant women. We conducted model simulations to investigate the combined physiological implications of low Mg^{2+} intake combined with either low or high Ca^{2+} diet (model predictions summarized in Figure 11). Model predictions indicated that reduced dietary Ca^{2+} intake may improve serum Mg^{2+} levels; although plasma Ca^{2+}, which is suppressed in Mg^{2+} deficiency, would be even lower as expected (Figure 7). In contrast, increased dietary Ca^{2+} intake raises serum Ca^{2+} levels, which inhibits PTH secretion and $1,25(OH)_2D_3$ synthesis, suppressing the resorption of Mg^{2+} from the slow bone pool, intestinal Mg^{2+} absorption, and renal reabsorption. Thus, higher dietary Ca^{2+} intake may exacerbate hypomagnesemia (Figure 7).

Mg^{2+} and Ca^{2+} homeostasis is altered in chronic kidney disease, even though the kidneys undergo adaptations such that hypermagnesemia and hypocalcemia are not observed until advanced chronic kidney disease. Mg^{2+} deficiency can be associated with abnormal vitamin D function. Indeed, chronic kidney disease is one of the main conditions associated with low 25(OH)D serum levels, with the vast majority of

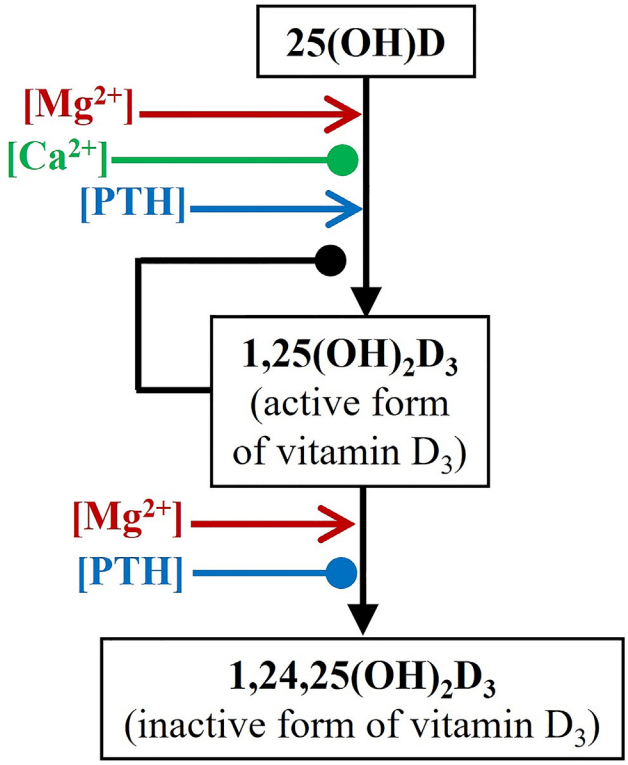

Figure 8. Schematic of the regulation of different forms of vitamin D_3 by Mg^{2+}, Ca^{2+}, PTH, and $1,25(OH)_2D_3$
Arrows denote activation and closed circles denote inhibition.

patients with chronic kidney disease exhibiting vitamin D insufficiency (>80% of cases[60,61]). The known causes and risk factors for vitamin D insufficiency include age,[62] female sex,[60] proteinuria,[62] diabetes,[63] and impaired 25(OH)D tubular reabsorption.[64]

Our simulations results (summarized in Figure 11) suggested that deficiency of $1,25(OH)_2D_3$ has a critical role in maintaining Ca^{2+} homeostasis as its deficiency can cause severe hypocalcemia.[49] In contrast, deficiency of $1,25(OH)_2D_3$ was not predicted to severely impact Mg^{2+} homeostasis, even though low $1,25(OH)_2D_3$ levels may reduce intestinal Mg^{2+} absorption in patients with chronic kidney disease. Interestingly, patients with advanced chronic kidney disease (estimated glomerular filtration rate (eGFR) <30 mL/min) were observed to develop hypermagnesemia not hypomagnesemia. That is due to the drastically reduced filtered Mg^{2+} and thus Mg^{2+} excretion, despite an increase in fractional excretion of Mg^{2+}. While our simulations of $1,25(OH)_2D_3$ deficiency was motivated by the impacts of chronic kidney disease on Ca^{2+} and Mg^{2+} homeostasis, they did not represent impairment in kidney function and thus predicted a drop in plasma Mg^{2+} in advanced chronic kidney disease rather than hypermagnesemia (Figure 9).

In summary, we have developed a computational model of Mg^{2+} and Ca^{2+} homeostasis and their regulation by the calciotropic hormones, PTH and $1,25(OH)_2D_3$, in a male rat. The model was used to understand the underlying mechanisms involved in regulating Mg^{2+} and Ca^{2+} balance during dietary Mg^{2+} deficiency, low/high dietary Ca^{2+} with Mg^{2+} deficiency, and vitamin D_3 deficiency.

Limitations of the study

Substantial efforts have been invested in understanding the sex differences in Ca^{2+} regulation and balance.[4,65–68] In contrast, much less is known about the sex differences in Mg^{2+} homeostasis, with no sex differences reported in serum Mg^{2+} levels.[69,70] That said, urinary Mg^{2+} excretion appears to be higher in men,[71] an observation that may stem, at least in part, from differences in kidney structure and function between the two sexes. In rodent studies, Veiras et al. characterized major differences in transport capacities across tubular nephron segments in male and female rat kidneys.[72] Specifically, in the proximal tubule, female rats exhibit heightened NHE3 phosphorylation and relocation to the base of microvilli, where activity is reduced compared to male rats. Consequently, the proximal tubule of female rats reabsorbs a notably smaller portion of filtered Na^+ in comparison to male rats. Because proximal tubular Mg^{2+} transport is linked to Na^+ transport, a modeling study[73] predicted that the proximal tubule of female rats also reabsorbs a smaller fraction of filtered Mg^{2+} compared to males. The present model is based primarily on a male rat. A worthwhile extension is to develop sex-specific models for whole-body Ca^{2+} and Mg^{2+} regulation, in health and diseases (e.g., chronic kidney disease). In addition, age is also an important factor in Mg^{2+} homeostasis. Aging is often associated with Mg^{2+} deficiency which can result from reduced intestinal absorption, increased urinary excretion due to reduction in kidney function, or inadequate dietary Mg^{2+} intake.[56] Developing age-specific models will help us better understand the mechanisms involved in Mg^{2+}

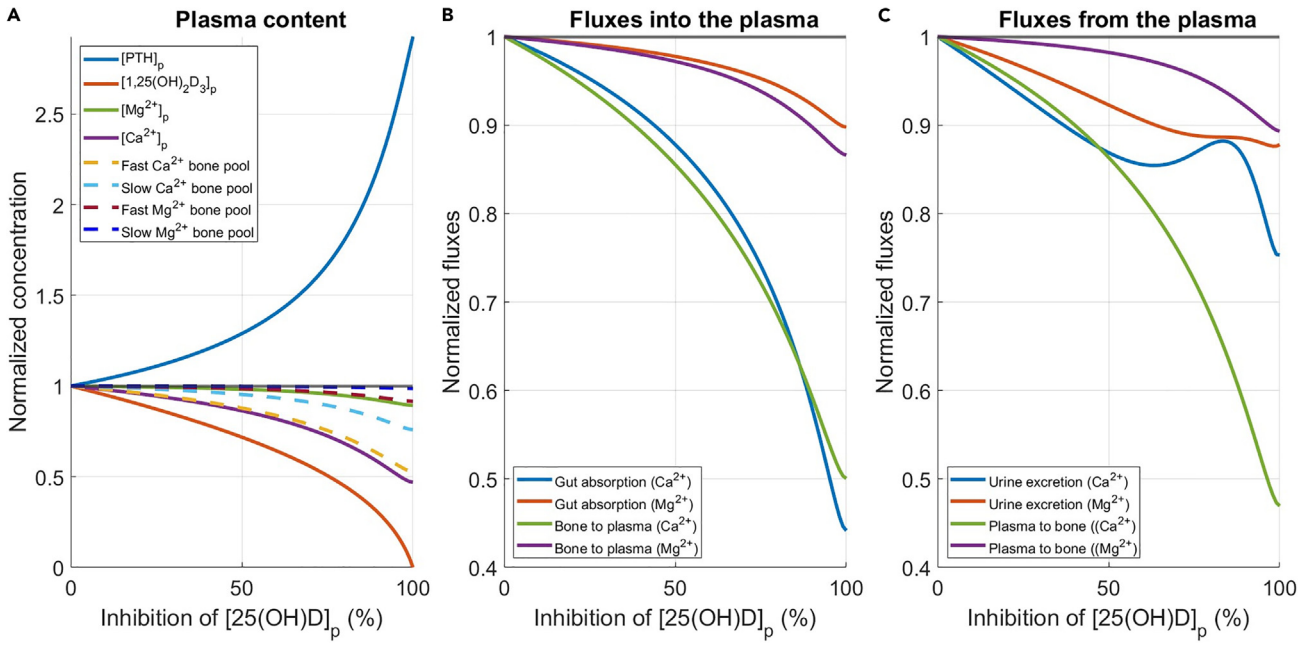

Figure 9. Inactive vitamin D3 (25(OH)D) deficiency

Predicted normalized steady state plasma concentrations and fluxes at decreased $[25(OH)D]_p$

(A–C) All y axis values are normalized to the baseline values. (A) Normalized steady state plasma concentrations of PTH, $1,25(OH)_2D_3$, Ca^{2+}, and Mg^{2+}. (B) Normalized steady state Mg^{2+} and Ca^{2+} fluxes into plasma. (C) Normalized steady state Mg^{2+} and Ca^{2+} fluxes out of plasma.

dyshomeostasis in old age. Another limitation of this model is the data used to estimate the parameters; for instance, parameters representing fractional intestinal absorption of Mg^{2+} were obtained from studies conducted on humans. Also, the model describes transport and regulation mechanisms at the cellular level in the kidneys and intestine by means of simplified relationships, such as first-order kinetics and Michaelis-Menten equations. We have developed detailed epithelial cell-based models of Ca^{2+} and Mg^{2+} transport in a rat kidney[65,73]; these could be integrated in the present mathematical model in the future. In addition, Mg^{2+} plays an important role in bone remodeling. Mg^{2+} increases osteoblast proliferation and its deficiency causes increased osteoclast formation and release of inflammatory cytokines leading

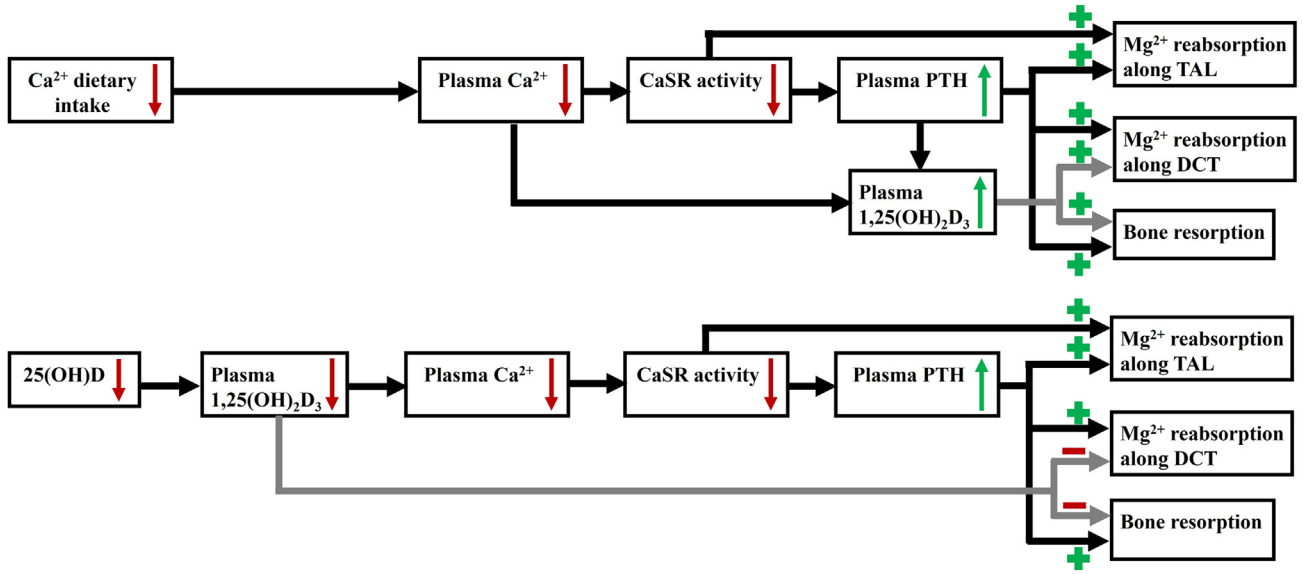

Figure 10. Summary of changes in response to dietary Ca^{2+} restriction and 25(OH)D inhibition

Downward red arrows indicate decrease and upward green arrows indicate increase. Arrows with the green plus sign (+) indicate activation and arrows with the red minus sign (–) indicate inhibition. TAL, thick ascending limb; DCT, distal convoluted tubule.

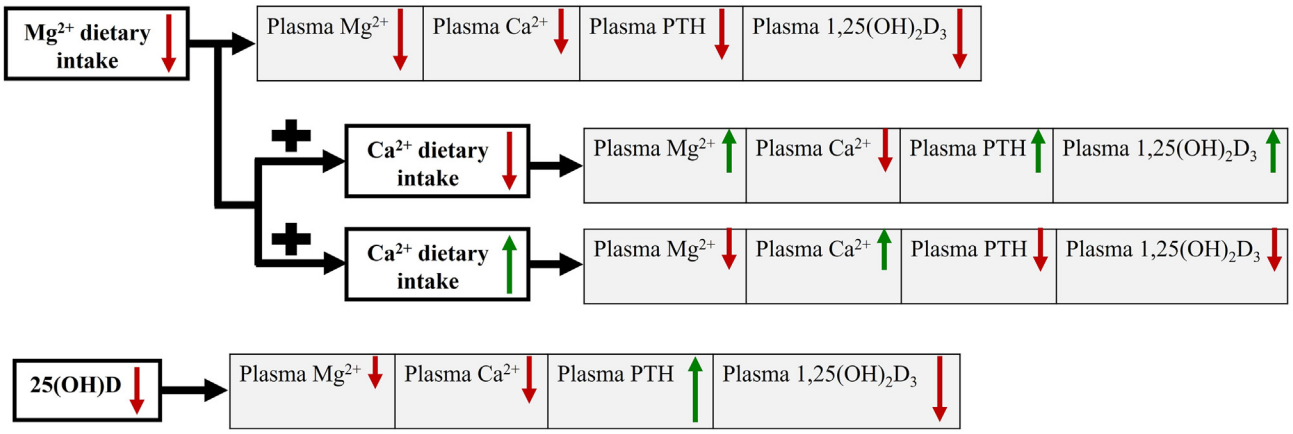

Figure 11. Summarized predicted changes in plasma concentrations of Mg^{2+}, Ca^{2+}, PTH, and $1,25(OH)_2D_3$ in the presence of (i) dietary Mg^{2+} deficiency, (ii) low/high dietary Ca^{2+} in the presence of dietary Mg^{2+} deficiency, and (iii) 25(OH)D deficiency

Arrow lengths are representative of the extent of change. Downward red arrows indicate decrease and upward green arrows indicate increase.

to significant bone loss.[74,75] Developing a detailed model of bone remodeling by considering the impact of Mg^{2+} on bone resorption and formation may shed light into why severe dietary Mg^{2+} deficiency results in hypercalcemia in rodents and hypocalcemia in other species.

RESOURCE AVAILABILITY

Lead contact

Further information and requests for resources should be directed to the lead contact, Pritha Dutta (p7dutta@uwaterloo.ca).

Materials availability

This study did not generate new unique reagents or other new materials.

Data and code availability

The code generated in this study can be accessed at https://github.com/Pritha17/Magnesium_calcium_homeostasis.[76]

ACKNOWLEDGMENTS

This work was supported by the Canada 150 Research Chair program, National Sciences and Engineering Research Council of Canada (NSERC) Discovery Grant (RGPIN-2019-03916), and Canadian Institutes of Health Research (CIHR) Project grant (TNC-174963) to A.T.L.

AUTHOR CONTRIBUTIONS

Conceptualization, P.D. and A.T.L.; methodology, P.D. and A.T.L.; software, validation, formal analysis, and investigation, P.D.; resources, A.T.L.; data curation, P.D.; writing – original draft, P.D. and A.T.L; writing – review and editing, P.D. and A.T.L.; visualization, P.D.; supervision, P.D. and A.T.L.; funding acquisition, A.T.L.

DECLARATION OF INTERESTS

The authors declare no competing interests.

STAR★METHODS

Detailed methods are provided in the online version of this paper and include the following:

- KEY RESOURCES TABLE
- METHOD DETAILS
  - Parathyroid gland and parathyroid hormone
  - Plasma $1,25(OH)_2D_3$
  - Proximal tubule of the kidney
  - Thick ascending limb of the kidney
  - Distal convoluted tubule of the kidney
  - Intestine
  - Bones
  - Plasma magnesium
- QUANTIFICATION AND STATISTICAL ANALYSIS

Received: May 14, 2024
Revised: August 21, 2024
Accepted: September 27, 2024
Published: September 30, 2024

REFERENCES

1. Taal, M.W., Chertow, G.M., Marsden, P.A., Skorecki, K., Alan, S., and Brenner, B.M. (2011). Brenner and Rector's the Kidney E-Book (Elsevier Health Sciences).
2. Institute of Medicine (US) Standing Committee on the Scientific Evaluation of Dietary Reference Intakes (1997). Dietary Reference Intakes for Calcium, Phosphorus, Magnesium, Vitamin D, and Fluoride (National Academies Press). (US).
3. Granjon, D., Bonny, O., and Edwards, A. (2016). A model of calcium homeostasis in the rat. Am. J. Physiol. Renal Physiol. *311*, F1047–F1062. https://doi.org/10.1152/ajprenal.00230.2016.
4. Stadt, M.M., and Layton, A.T. (2023). Mathematical modeling of calcium homeostasis in female rats: An analysis of sex differences and maternal adaptations. J. Theor. Biol. *572*, 111583. https://doi.org/10.1016/j.jtbi.2023.111583.
5. Bichara, M., Mercier, O., Borensztein, P., and Paillard, M. (1990). Acute metabolic acidosis enhances circulating parathyroid hormone, which contributes to the renal response against acidosis in the rat. J. Clin. Invest. *86*, 430–443. https://doi.org/10.1172/JCI114729.
6. Fox, J. (1991). Regulation of parathyroid hormone secretion by plasma calcium in aging rats. Am. J. Physiol. *260*, E220–E225. https://doi.org/10.1152/ajpendo.1991.260.2.E220.
7. Bushinsky, D.A., Riera, G.S., Favus, M.J., and Coe, F.L. (1985). Evidence that blood ionized calcium can regulate serum 1, 25 (OH) 2D3 independently of parathyroid hormone and phosphorus in the rat. J. Clin. Invest. *76*, 1599–1604. https://doi.org/10.1172/JCI112143.
8. Gray, R.W. (1981). Control of plasma 1, 25-(OH) 2-vitamin D concentrations by calcium and phosphorus in the rat: effects of hypophysectomy. Calcif. Tissue Int. *33*, 485–488. https://doi.org/10.1007/BF02409478.
9. Rude, R.K., Gruber, H.E., Norton, H.J., Wei, L.Y., Frausto, A., and Kilburn, J. (2006). Reduction of dietary magnesium by only 50% in the rat disrupts bone and mineral metabolism. Osteoporos. Int. *17*, 1022–1032. https://doi.org/10.1007/s00198-006-0104-3.
10. Altura, B.M., Shah, N.C., Li, Z., Jiang, X.-C., Perez-Albela, J.L., and Altura, B.T. (2010). Magnesium deficiency upregulates serine palmitoyl transferase (SPT 1 and SPT 2) in cardiovascular tissues: relationship to serum ionized Mg and cytochrome c. Am. J. Physiol. Heart Circ. Physiol. *299*, H932–H938. https://doi.org/10.1152/ajpheart.01076.2009.
11. Jeong, S.M., Hahm, K.D., Shin, J.W., Leem, J.G., Lee, C., and Han, S.M. (2006). Changes in magnesium concentration in the serum and cerebrospinal fluid of neuropathic rats. Acta Anaesthesiol. Scand. *50*, 211–216. https://doi.org/10.1111/j.1399-6576.2006.00925.x.
12. Bassani, R.A., Gilioli, R., Oliveira, E.S., and Hoehr, N.F. (2012). Blood calcium levels in immature rats: influence of extracellular calcium concentration on myocardial calcium handling. Exp. Anim. *61*, 399–405. https://doi.org/10.1538/expanim.61.399.
13. Coudray, C., Feillet-Coudray, C., Grizard, D., Tressol, J.C., Gueux, E., and Rayssiguier, Y. (2002). Fractional intestinal absorption of magnesium is directly proportional to dietary magnesium intake in rats. J. Nutr. *132*, 2043–2047. https://doi.org/10.1093/jn/132.7.2043.
14. Quitterer, U., Hoffmann, M., Freichel, M., and Lohse, M.J. (2001). Paradoxical block of parathormone secretion is mediated by increased activity of Gα subunits. J. Biol. Chem. *276*, 6763–6769. https://doi.org/10.1074/jbc.M007727200.
15. Quamme, G.A., and Dirks, J.H. (1986). The physiology of renal magnesium handling. Kidney Blood Press Res. *9*, 257–269. https://doi.org/10.1159/000173090.
16. Brown, E.M., and Chen, C.J. (1989). Calcium, magnesium and the control of PTH secretion. Bone Miner. *5*, 249–257. https://doi.org/10.1016/0169-6009(89)90003-2.
17. Sadick, M., Attenberger, U., Kraenzlin, B., Kayed, H., Schoenberg, S.O., Gretz, N., and Schock-Kusch, D. (2011). Two non-invasive GFR-estimation methods in rat models of polycystic kidney disease: 3.0 Tesla dynamic contrast-enhanced MRI and optical imaging. Nephrol. Dial. Transplant. *26*, 3101–3108. https://doi.org/10.1093/ndt/gfr148.
18. Hardwick, L.L., Jones, M.R., Brautbar, N., and Lee, D.B. (1991). Magnesium absorption: mechanisms and the influence of vitamin D, calcium and phosphate. J. Nutr. *121*, 13–23. https://doi.org/10.1093/jn/121.1.13.
19. Jahnen-Dechent, W., and Ketteler, M. (2012). Magnesium basics. Clin. Kidney J. *5*, i3–i14. https://doi.org/10.1093/ndtplus/sfr163.
20. Sobol', I.M. (1990). On sensitivity estimation for nonlinear mathematical models. Mat. Model. *2*, 112–118.
21. DiNicolantonio, J.J., O'Keefe, J.H., and Wilson, W. (2018). Subclinical magnesium deficiency: a principal driver of cardiovascular disease and a public health crisis. Open Heart *5*, e000668. https://doi.org/10.1136/openhrt-2017-000668.
22. Costello, R.B., Elin, R.J., Rosanoff, A., Wallace, T.C., Guerrero-Romero, F., Hruby, A., Lutsey, P.L., Nielsen, F.H., Rodriguez-Moran, M., Song, Y., and Van Horn, L.V. (2016). Perspective: the case for an evidence-based reference interval for serum magnesium: the time has come. Adv. Nutr. *7*, 977–993. https://doi.org/10.3945/an.116.012765.
23. Risco, F., and Traba, M.L. (1992). Influence of magnesium on the *in vitro* synthesis of 24, 25-dihydroxyvitamin D3 and 1 alpha, 25-dihydroxyvitamin D3. Magnes. Res. *5*, 5–14.
24. Matsuzaki, H., Katsumata, S.i., Kajita, Y., and Miwa, M. (2013). Magnesium deficiency regulates vitamin D metabolizing enzymes and type II sodium-phosphate cotransporter mRNA expression in rats. Magnes. Res. *26*, 83–86. https://doi.org/10.1684/mrh.2013.0341.
25. Rude, R.K., Gruber, H.E., Norton, H.J., Wei, L.Y., Frausto, A., and Kilburn, J. (2005). Dietary magnesium reduction to 25% of nutrient requirement disrupts bone and mineral metabolism in the rat. Bone *37*, 211–219. https://doi.org/10.1016/j.bone.2005.04.005.
26. Rude, R.K., Gruber, H.E., Norton, H.J., Wei, L.Y., Frausto, A., and Mills, B.G. (2004). Bone loss induced by dietary magnesium reduction to 10% of the nutrient requirement in rats is associated with increased release of substance P and tumor necrosis factor-α. J. Nutr. *134*, 79–85. https://doi.org/10.1093/jn/134.1.79.
27. Fong, J., and Khan, A. (2012). Hypocalcemia: updates in diagnosis and management for primary care. Can. Fam. Physician *58*, 158–162.
28. Swaminathan, R. (2003). Magnesium metabolism and its disorders. Clin. Biochem. Rev. *24*, 47–66.
29. Rude, R.K., Gruber, H.E., Wei, L.Y., Frausto, A., and Mills, B.G. (2003). Magnesium deficiency: effect on bone and mineral metabolism in the mouse. Calcif. Tissue Int. *72*, 32–41. https://doi.org/10.1007/s00223-001-1091-1.
30. Jones, J.E., Schwartz, R., and Krook, L. (1980). Calcium homeostasis and bone pathology in magnesium deficient rats. Calcif. Tissue Int. *31*, 231–238. https://doi.org/10.1007/BF02407186.
31. Larvor, P., and Labat, M.-L. (1978). The influence of magnesium deficiency on calcium metabolism in the rat. In Annales de Biologie Animale Biochimie Biophysique (EDP Sciences), pp. 149–155.
32. Fatemi, S., Ryzen, E., Flores, J., Endres, D.B., and Rude, R.K. (1991). Effect of experimental human magnesium depletion on parathyroid hormone secretion and 1, 25-dihydroxyvitamin D metabolism. J. Clin. Endocrinol. Metab. *73*, 1067–1072. https://doi.org/10.1210/jcem-73-5-1067.
33. Creedon, A., Flynn, A., and Cashman, K. (1999). The effect of moderately and severely restricted dietary magnesium intakes on bone composition and bone metabolism in the rat. Br. J. Nutr. *82*, 63–71. https://doi.org/10.1017/S0007114599001130.
34. Castiglioni, S., Cazzaniga, A., Albisetti, W., and Maier, J.A.M. (2013). Magnesium and osteoporosis: current state of knowledge and future research directions. Nutrients *5*, 3022–3033. https://doi.org/10.3390/nu5083022.
35. Welsh, J.J., and Weaver, V.M. (1988). Adaptation to low dietary calcium in magnesium-deficient rats. J. Nutr. *118*, 729–734. https://doi.org/10.1093/jn/118.6.729.
36. Bertinato, J., Lavergne, C., Plouffe, L.J., and El Niaj, H.A. (2014). Small increases in dietary calcium above normal requirements exacerbate magnesium deficiency in rats fed a low magnesium diet. Magnes. Res. *27*, 35–47. https://doi.org/10.1684/mrh.2014.0360.
37. Rosanoff, A., Weaver, C.M., and Rude, R.K. (2012). Suboptimal magnesium status in the

United States: are the health consequences underestimated? Nutr. Rev. *70*, 153–164. https://doi.org/10.1111/j.1753-4887.2011.00465.x.

38. Lewis, N.M., Marcus, M.S., Behling, A.R., and Greger, J.L. (1989). Calcium supplements and milk: effects on acid-base balance and on retention of calcium, magnesium, and phosphorus. Am. J. Clin. Nutr. *49*, 527–533. https://doi.org/10.1093/ajcn/49.3.527.
39. Seelig, M.S. (1964). The requirement of magnesium by the normal adult: summary and analysis of published data. Am. J. Clin. Nutr. *14*, 242–290. https://doi.org/10.1093/ajcn/14.6.342.
40. Putz-Bankuti, C., Pilz, S., Stojakovic, T., Scharnagl, H., Pieber, T.R., Trauner, M., Obermayer-Pietsch, B., and Stauber, R.E. (2012). Association of 25-hydroxyvitamin D levels with liver dysfunction and mortality in chronic liver disease. Liver Int. *32*, 845–851. https://doi.org/10.1111/j.1478-3231.2011.02735.x.
41. Arteh, J., Narra, S., and Nair, S. (2010). Prevalence of vitamin D deficiency in chronic liver disease. Dig. Dis. Sci. *55*, 2624–2628. https://doi.org/10.1007/s10620-009-1069-9.
42. Malham, M., Jørgensen, S.P., Ott, P., Agnholt, J., Vilstrup, H., Borre, M., and Dahlerup, J.F. (2011). Vitamin D deficiency in cirrhosis relates to liver dysfunction rather than aetiology. World J. Gastroenterol. *17*, 922. https://doi.org/10.3748/wjg.v17.i7.922.
43. Restrepo Valencia, C.A., and Aguirre Arango, J.V. (2016). Vitamin D (25 (OH) D) in patients with chronic kidney disease stages 2-5. Colomb. Méd. *47*, 160–166.
44. Dusso, A., González, E.A., and Martin, K.J. (2011). Vitamin D in chronic kidney disease. Best Pract. Res. Clin. Endocrinol. Metab. *25*, 647–655. https://doi.org/10.1016/j.beem.2011.05.005.
45. Heaney, R.P., Dowell, M.S., Hale, C.A., and Bendich, A. (2003). Calcium absorption varies within the reference range for serum 25-hydroxyvitamin D. J. Am. Coll. Nutr. *22*, 142–146. https://doi.org/10.1080/07315724.2003.10719287.
46. Wassner, S.J., Li, J.B., Sperduto, A., and Norman, M.E. (1983). Vitamin D Deficiency, hypocalcemia, and increased skeletal muscle degradation in rats. J. Clin. Invest. *72*, 102–112. https://doi.org/10.1172/JCI110947.
47. Yamamoto, M., Kawanobe, Y., Takahashi, H., Shimazawa, E., Kimura, S., and Ogata, E. (1984). Vitamin D deficiency and renal calcium transport in the rat. J. Clin. Invest. *74*, 507–513. https://doi.org/10.1172/JCI111448.
48. Metzger, M., Houillier, P., Gauci, C., Haymann, J.P., Flamant, M., Thervet, E., Boffa, J.-J., Vrtovsnik, F., Froissart, M., Stengel, B., et al. (2013). Relation between circulating levels of 25 (OH) vitamin D and parathyroid hormone in chronic kidney disease: quest for a threshold. J. Clin. Endocrinol. Metab. *98*, 2922–2928. https://doi.org/10.1210/jc.2013-1294.
49. Agus, Z.S., Wasserstein, A., and Goldfarb, S. (1982). Disorders of calcium and magnesium homeostasis. Am. J. Med. *72*, 473–488. https://doi.org/10.1016/0002-9343(82)90519-8.
50. Marier, J.R. (1986). Magnesium content of the food supply in the modern-day world. Magnesium *5*, 1–8.
51. de Baaij, J.H.F. (2023). Magnesium reabsorption in the kidney. Am. J. Physiol. Renal Physiol. *324*, F227–F244. https://doi.org/10.1152/ajprenal.00298.2022.
52. Wong, E.T., Rude, R.K., Singer, F.R., and Shaw, S.T., Jr. (1983). A high prevalence of hypomagnesemia and hypermagnesemia in hospitalized patients. Am. J. Clin. Pathol. *79*, 348–352. https://doi.org/10.1093/ajcp/79.3.348.
53. Yano, K., Heilbrun, L.K., Wasnich, R.D., Hankin, J.H., and Vogel, J.M. (1985). The relationship between diet and bone mineral content of multiple skeletal sites in elderly Japanese-American men and women living in Hawaii. Am. J. Clin. Nutr. *42*, 877–888. https://doi.org/10.1093/ajcn/42.5.877.
54. New, S.A., Robins, S.P., Campbell, M.K., Martin, J.C., Garton, M.J., Bolton-Smith, C., Grubb, D.A., Lee, S.J., and Reid, D.M. (2000). Dietary influences on bone mass and bone metabolism: further evidence of a positive link between fruit and vegetable consumption and bone health? Am. J. Clin. Nutr. *71*, 142–151. https://doi.org/10.1093/ajcn/71.1.142.
55. Tucker, K.L., Hannan, M.T., Chen, H., Cupples, L.A., Wilson, P.W., and Kiel, D.P. (1999). Potassium, magnesium, and fruit and vegetable intakes are associated with greater bone mineral density in elderly men and women. Am. J. Clin. Nutr. *69*, 727–736. https://doi.org/10.1093/ajcn/69.4.727.
56. Barbagallo, M., Belvedere, M., and Dominguez, L.J. (2009). Magnesium homeostasis and aging. Magnes. Res. *22*, 235–246. https://doi.org/10.1684/mrh.2009.0187.
57. Kemter, E., Rathkolb, B., Bankir, L., Schrewe, A., Hans, W., Landbrecht, C., Klaften, M., Ivandic, B., Fuchs, H., Gailus-Durner, V., et al. (2010). Mutation of the Na+-K+-2Cl- cotransporter NKCC2 in mice is associated with severe polyuria and a urea-selective concentrating defect without hyperreninemia. Am. J. Physiol. Renal Physiol. *298*, F1405–F1415. https://doi.org/10.1152/ajprenal.00522.2009.
58. Nijenhuis, T., Vallon, V., van der Kemp, A.W.C.M., Loffing, J., Hoenderop, J.G.J., and Bindels, R.J.M. (2005). Enhanced passive Ca 2+ reabsorption and reduced Mg 2+ channel abundance explains thiazide-induced hypocalciuria and hypomagnesemia. J. Clin. Invest. *115*, 1651–1658. https://doi.org/10.1172/JCI24134.
59. Shlisky, J., Mandlik, R., Askari, S., Abrams, S., Belizan, J.M., Bourassa, M.W., Cormick, G., Driller-Colangelo, A., Gomes, F., Khadilkar, A., et al. (2022). Calcium deficiency worldwide: Prevalence of inadequate intakes and associated health outcomes. Ann. N. Y. Acad. Sci. *1512*, 10–28. https://doi.org/10.1111/nyas.14758.
60. Filipov, J.J., Zlatkov, B.K., Dimitrov, E.P., and Svinarov, D. (2015). Relationship between vitamin D status and immunosuppressive therapy in kidney transplant recipients. Biotechnol. Biotechnol. Equip. *29*, 331–335. https://doi.org/10.1080/13102818.2014.995415.
61. Ngai, M., Lin, V., Wong, H.C., Vathsala, A., and How, P. (2014). Vitamin D status and its association with mineral and bone disorder in a multi-ethnic chronic kidney disease population. Clin. Nephrol. *82*, 231–239. https://doi.org/10.5414/cn108182.
62. Caravaca-Fontán, F., Gonzales-Candia, B., Luna, E., and Caravaca, F. (2016). Relative importance of the determinants of serum levels of 25-hydroxy vitamin D in patients with chronic kidney disease. Nefrol. Engl. Ed. *36*, 510–516. https://doi.org/10.1016/j.nefroe.2016.11.010.
63. Mohiuddin, S.A., Marie, M., Ashraf, M., Hussein, M., and Almalki, N. (2016). Is there an association between Vitamin D level and inflammatory markers in hemodialysis patients? A cross-sectional study. Saudi J. Kidney Dis. Transpl. *27*, 460–466. https://doi.org/10.4103/1319-2442.182377.
64. Takemoto, F., Shinki, T., Yokoyama, K., Inokami, T., Hara, S., Yamada, A., Kurokawa, K., and Uchida, S. (2003). Gene expression of vitamin D hydroxylase and megalin in the remnant kidney of nephrectomized rats. Kidney Int. *64*, 414–420. https://doi.org/10.1046/j.1523-1755.2003.00114.x.
65. Hakimi, S., Dutta, P., and Layton, A.T. (2023). Coupling of renal sodium and calcium transport: A modeling analysis of transporter inhibition and sex differences. Am. J. Physiol. Renal Physiol. *325*, F536–F551. https://doi.org/10.1152/ajprenal.00145.2023.
66. Okano, T., Kimura, T., Tsugawa, N., Okamura, Y., and Kobayashi, T. (1994). Roles of parathyroid hormone and 1α, 25-dihydroxyvitamin D 3 in bone growth of growing male and female rats. J. Bone Miner. Metab. *12*, S23–S26. https://doi.org/10.1007/BF02375670.
67. Song, Y., and Fleet, J.C. (2004). 1, 25 dihydroxycholecalciferol-mediated calcium absorption and gene expression are higher in female than in male mice. J. Nutr. *134*, 1857–1861. https://doi.org/10.1093/jn/134.8.1857.
68. Khalil, R., Kim, N.R., Jardi, F., Vanderschueren, D., Claessens, F., and Decallonne, B. (2018). Sex steroids and the kidney: role in renal calcium and phosphate handling. Mol. Cell. Endocrinol. *465*, 61–72. https://doi.org/10.1016/j.mce.2017.11.011.
69. Jagarinec, N., Flegar-Meštrić, Z., Šurina, B., Vrhovski-Hebrang, D., and Preden-Kereković, V. (1998). Pediatric Reference Intervals for 34 Biochemical Analytes in Urban School Children and Adolescents. Clin Chem Lab Med. *36*, 327–337. https://doi.org/10.1515/CCLM.1998.055.
70. Bohnen, N., Degenaar, C., and Jolles, J. (1991). Influence of age and sex on 19 blood variables in healthy subjects. Z. Gerontol. *24*, 339–345.
71. Jankûnas, R., Driþienë, Z., Stakiðaitis, D., and Kulieðienë, I. (2001). Gender-dependent Magnesium Urinary Excretion in Healthy Adolescents and Adults. Acta Med. Litu. *8*, 167–172.
72. Veiras, L.C., Girardi, A.C.C., Curry, J., Pei, L., Ralph, D.L., Tran, A., Castelo-Branco, R.C., Pastor-Soler, N., Arranz, C.T., Yu, A.S.L., and McDonough, A.A. (2017). Sexual Dimorphic Pattern of Renal Transporters and Electrolyte Homeostasis. J. Am. Soc. Nephrol. *28*, 3504–3517. https://doi.org/10.1681/ASN.2017030295.
73. Dutta, P., Hakimi, S., and Layton, A.T. (2024). How the kidney regulates magnesium: a modelling study. R. Soc. Open Sci. *11*, 231484. https://doi.org/10.1098/rsos.231484.
74. Belluci, M.M., Schoenmaker, T., Rossa-Junior, C., Orrico, S.R., de Vries, T.J., and Everts, V. (2013). Magnesium deficiency results in an increased formation of osteoclasts. J. Nutr. Biochem. *24*, 1488–1498. https://doi.org/10.1016/j.jnutbio.2012.12.008.
75. Mazur, A., Maier, J.A.M., Rock, E., Gueux, E., Nowacki, W., and Rayssiguier, Y. (2007). Magnesium and the inflammatory response: potential physiopathological implications.

Arch. Biochem. Biophys. *458*, 48–56. https://doi.org/10.1016/j.abb.2006.03.031.
76. Dutta, P. (2024). Pritha17/Magnesium_calcium_homeostasis: v1.0.0 (v1.0.0). Zenodo. https://doi.org/10.5281/zenodo.13787641.
77. Ferre, S., Hoenderop, J.G., and Bindels, R.J. (2012). Sensing mechanisms involved in Ca2+ and Mg2+ homeostasis. Kidney Int. *82*, 1157–1166. https://doi.org/10.1038/ki.2012.179.
78. Habener, J.F., and Potts, J.T. (1976). Relative effectiveness of magnesium and calcium on the secretion and biosynthesis of parathyroid hormone *in vitro*. Endocrinology *98*, 197–202. https://doi.org/10.1210/endo-98-1-197.
79. Ruat, M., Snowman, A.M., Hester, L.D., and Snyder, S.H. (1996). Cloned and Expressed Rat Ca2+-sensing Receptor: DIFFERENTIAL COOPERATIVE RESPONSES TO CALCIUM AND MAGNESIUM (*). J. Biol. Chem. *271*, 5972–5975. https://doi.org/10.1074/jbc.271.11.5972.
80. Bräuner-Osborne, H., Jensen, A.A., Sheppard, P.O., O'Hara, P., and Krogsgaard-Larsen, P. (1999). The Agonist-binding Domain of the Calcium-sensing Receptor Is Located at the Amino-terminal Domain. J. Biol. Chem. *274*, 18382–18386. https://doi.org/10.1074/jbc.274.26.18382.
81. Rodríguez-Ortiz, M.E., Canalejo, A., Herencia, C., Martínez-Moreno, J.M., Peralta-Ramírez, A., Perez-Martinez, P., Navarro-González, J.F., Rodríguez, M., Peter, M., Gundlach, K., et al. (2014). Magnesium modulates parathyroid hormone secretion and upregulates parathyroid receptor expression at moderately low calcium concentration. Nephrol. Dial. Transplant. *29*, 282–289. https://doi.org/10.1093/ndt/gft400.
82. Silver, J., Naveh-Many, T., Mayer, H., Schmelzer, H.J., and Popovtzer, M.M. (1986). Regulation by vitamin D metabolites of parathyroid hormone gene transcription *in vivo* in the rat. J. Clin. Invest. *78*, 1296–1301. https://doi.org/10.1172/JCI112714.
83. Vetter, T., and Lohse, M.J. (2002). Magnesium and the parathyroid. Curr. Opin. Nephrol. Hypertens. *11*, 403–410. https://doi.org/10.1097/00041552-200207000-00006.
84. Uwitonze, A.M., and Razzaque, M.S. (2018). Role of magnesium in vitamin D activation and function. J. Osteopath. Med. *118*, 181–189. https://doi.org/10.7556/jaoa.2018.037.
85. Curry, J.N., and Yu, A.S.L. (2018). Magnesium Handling in the Kidney. Adv. Chronic Kidney Dis. *25*, 236–243. https://doi.org/10.1053/j.ackd.2018.01.003.
86. Dai, L.-J., Ritchie, G., Kerstan, D., Kang, H.S., Cole, D.E., and Quamme, G.A. (2001). Magnesium transport in the renal distal convoluted tubule. Physiol. Rev. *81*, 51–84. https://doi.org/10.1152/physrev.2001.81.1.51.
87. Quamme, G.A. (2008). Recent developments in intestinal magnesium absorption. Curr. Opin. Gastroenterol. *24*, 230–235. https://doi.org/10.1097/MOG.0b013e3282f37b59.
88. Wallach, S. (1990). Effects of magnesium on skeletal metabolism. Magnes. Trace. Elem. *9*, 1–14.
89. Silva, B.C., and Bilezikian, J.P. (2015). Parathyroid hormone: anabolic and catabolic actions on the skeleton. Curr. Opin. Pharmacol. *22*, 41–50. https://doi.org/10.1016/j.coph.2015.03.005.
90. Takahashi, N., Udagawa, N., and Suda, T. (2014). Vitamin D endocrine system and osteoclasts. BoneKEy Rep. *3*, 495. https://doi.org/10.1038/bonekey.2013.229.

STAR★METHODS

KEY RESOURCES TABLE

REAGENT or RESOURCE	SOURCE	IDENTIFIER
Software and algorithms		
Computer code	This study	https://github.com/Pritha17/Magnesium_calcium_homeostasis (https://doi.org/10.5281/zenodo.13787641)

METHOD DETAILS

The Mg^{2+} homeostasis model consists of five compartments: plasma, intestine, kidney, parathyroid gland, and bone. The model equations in each compartment are described in the following sections. Model parameters are listed in Table 2. For model equations and parameters related to Ca^{2+} homeostasis refer to Refs.[3,4]

Parathyroid gland and parathyroid hormone

PTH secretion and plasma Ca^{2+} and Mg^{2+} levels are regulated by a feedback loop. As plasma Ca^{2+} and Mg^{2+} levels drop, it signals the parathyroid glands to secrete more PTH. PTH stimulates Ca^{2+} and Mg^{2+} reabsorption in the kidney, Ca^{2+} and Mg^{2+} absorption in the intestine, and bone resorption. All these actions increase plasma Ca^{2+} and Mg^{2+} concentrations. The increased levels of these two cations then serve as a negative feedback signal to the parathyroid glands to decrease PTH secretion.

Parathyroid cells sense extracellular Ca^{2+} and Mg^{2+} concentrations through the calcium-sensing receptors (CaSR) on their cell surface.[77] Ca^{2+} is the main agonist of CaSR and small changes in plasma Ca^{2+} concentration can induce rapid secretion of PTH.[78] At equimolar concentrations, Mg^{2+} is 1/2 to 2/3 as potent as Ca^{2+} in activating CaSR.[79,80] Mg^{2+} has different impacts on PTH secretion depending on the plasma Ca^{2+} concentration. The combined effect of Ca^{2+} and Mg^{2+} on PTH secretion, as reported in an *in vitro* study,[81] is represented by model equations as described below.

Change in PTH concentration in the parathyroid gland (PTH_g) is given by

$$\frac{d[PTH_g]}{dt} = \frac{k_{prod}^{PTHg}}{1+\gamma_{prod}^{1,25(OH)_2D_3}\left[1,25(OH)_2D_3\right]_p} - \left(k_{deg}^{PTHg} + F\left(\left[Ca^{2+}\right]_p, \left[Mg^{2+}\right]_p\right)\right)[PTH_g] \quad \text{(Equation 1)}$$

where k_{prod}^{PTHg} denotes the basal rate of PTH production in the parathyroid gland, $\gamma_{prod}^{1,25(OH)_2D_3}$ denotes the inhibition of PTH synthesis by $[1,25(OH)_2D_3]_p$, and k_{deg}^{PTHg} denotes the rate constant for PTH_g degradation. The first term on the right-hand-side of Equation 1 denotes the inhibition of PTH_g synthesis by $[1,25(OH)_2D_3]_p$ and is adopted from ref.[3] This term is based on the findings of Silver et al.[82] who found an exponentially decreasing relationship between the mRNA expression of the PTH precursor in parathyroid glands and the injected quantity of $1,25(OH)_2D_3$. $F([Ca^{2+}]_p, [Mg^{2+}]_p)$ models the exocytosis of PTH_g regulated by plasma Ca^{2+} and Mg^{2+} and is defined as

$$F\left(\left[Ca^{2+}\right]_p, \left[Mg^{2+}\right]_p\right) = h\left(\left[Mg^{2+}\right]_p\right) \times F1\left(\left[Ca^{2+}\right]_p, \left[Mg^{2+}\right]_p\right) + \left(1 - h\left(\left[Mg^{2+}\right]_p\right)\right) \times F2\left(\left[Mg^{2+}\right]_p\right) \quad \text{(Equation 2)}$$

where $h([Mg^{2+}]_p)$ controls the weightage given to each function and depends on the plasma Mg^{2+} concentration. The function $h([Mg^{2+}]_p)$ is defined as

$$h\left(\left[Mg^{2+}\right]_p\right) = \frac{\left(\frac{\left[Mg^{2+}\right]_p}{\left[Mg^{2+}\right]_{thres-PTH}}\right)^{50}}{1+\left(\frac{\left[Mg^{2+}\right]_p}{\left[Mg^{2+}\right]_{thres-PTH}}\right)^{50}} \quad \text{(Equation 3)}$$

where $[Mg^{2+}]_{thres-PTH}$ = 0.4 mM. The function $F1([Ca^{2+}]_p, [Mg^{2+}]_p)$ is defined as

$$F1\left(\left[Ca^{2+}\right]_p, \left[Mg^{2+}\right]_p\right) = \left(\frac{\gamma_{Ca}}{\left[Ca^{2+}\right]_p}\right)^{\gamma_p}\left(\beta_{exo}^{PTHg} - \frac{1}{1+\left(\frac{C_m}{\left[Mg^{2+}\right]_p}\right)^2}\right). \quad \text{(Equation 4)}$$

The above equation is formulated based on observations reported in ref.[81]:

1. Very high (>=5 mM) $[Mg^{2+}]_p$ inhibits PTH secretion at all $[Ca^{2+}]_p$.
2. At low or moderately low $[Ca^{2+}]_p$ (0.8-1 mM), $[Mg^{2+}]_p$ (0.5-2 mM) stimulates PTH secretion.
3. At normal $[Ca^{2+}]_p$ (1.2-1.25 mM), $[Mg^{2+}]_p$ (0.5-2 mM) does not have significant effect on PTH secretion; however, if $[Mg^{2+}]_p$ is very high (=5 mM), it inhibits PTH secretion.
4. At high $[Ca^{2+}]_p$ (=1.5 mM), $[Mg^{2+}]_p$ inhibits PTH secretion.

The parameter, β_{exo}^{PTHg}, denotes the maximal rate of PTH secretion from the parathyroid gland. $\left(\frac{\gamma_{Ca}}{[Ca^{2+}]_p}\right)^{\gamma_p}$ controls the maximum effect of $[Mg^{2+}]_p$ on PTH secretion at a specific $[Ca^{2+}]_p$, such that the lower the plasma Ca^{2+} concentration, the higher the maximum effect of $[Mg^{2+}]_p$ on PTH secretion. C_m controls the slope of the curve. The lower the Ca^{2+} concentration, the steeper the slope, a relation that reflects a significant effect of $[Mg^{2+}]_p$ on PTH secretion. The parameters β_{exo}^{PTHg}, γ_{Ca}, γ_p, and C_m were estimated by fitting to experimental data reported in ref.[81] and the comparison between model results and experimental data is given in Figure 2. All parameter descriptions and values are listed in Table 2.

The last term in Equation 2, $F2([Mg^{2+}]_p)$, is defined as

$$F2\left([Mg^{2+}]_p\right) = \frac{1}{1+\frac{K_{low-Mg}}{[Mg^{2+}]_p}}. \quad \text{(Equation 5)}$$

Equation 5 captures the following observation from ref.[83]: very low plasma $[Mg^{2+}]_p$ (<0.4 mM) inhibits PTH secretion at all $[Ca^{2+}]_p$.

The rate of change in plasma PTH concentration (PTH_p) is given by

$$\frac{d[PTH_p]}{dt} = F\left([Ca^{2+}]_p, [Mg^{2+}]_p\right)\frac{V_g}{V_p}[PTH_g] - k_{deg}^{PTH_p}[PTH_p] \quad \text{(Equation 6)}$$

where k_{deg}^{PTHp} denotes the rate of degradation of PTH_p. V_g and V_p denote the volumes of the parathyroid gland and plasma, respectively. The ratio $\frac{V_g}{V_p}$ takes into account the dilution of PTH in plasma.

Plasma $1,25(OH)_2D_3$

Dietary vitamin D_3 is first converted to 25-hydroxy vitamin D_3 (25(OH)D) by 25-hydroxylase in the liver.[84] 25(OH)D is then carried to the kidney, where it is either converted to the active form of vitamin D_3, 1,25-dihydroxy vitamin D_3 ($1,25(OH)_2D_3$), by 1α-hydroxylase or the inactive form, 24,25-dihydroxy vitamin D_3 ($24,25(OH)_2D_3$), by 24-hydroxylase.[84] Some of the $1,25(OH)_2D_3$ is converted to the inactive form, $1,24,25(OH)_2D_3$, by 24-hydroxylase.[84] The conversion from the inactive 25(OH)D to the active $1,25(OH)_2D_3$ is regulated by Mg^{2+}, Ca^{2+}, PTH, and $1,25(OH)_2D_3$ (Figure 8).

The plasma concentration of active $1,25(OH)_2D_3$ is given by

$$\frac{d[1,25(OH)_2D_3]_p}{dt} = \left[k_{conv}^{min} + \delta_{conv}^{max} \times f_{PTH-act} \times f_{CaSR-act} \times f_{1,25(OH)_2D_3-act} \times f_{Mg-act}\right][25(OH)D]_p - \left(k_{deg}^{1,25(OH)_2D_3} \times \left(f_{PTH-inact} + f_{Mg-inact}\right)\right)[1,25(OH)_2D_3]_p \quad \text{(Equation 7)}$$

where k_{conv}^{min} denotes the minimum production rate constant of $1,25(OH)_2D_3$, δ_{conv}^{max} denotes the maximum increase in $1,25(OH)_2D_3$ production rate, and $k_{deg}^{1,25(OH)_2D_3}$ denotes the degradation rate constant of $1,25(OH)_2D_3$. PTH promotes the production of $1,25(OH)_2D_3$ which is represented by $f_{PTH-act} = \frac{([PTH]_p)^{n_{conv}}}{(K_{conv}^{PTH})^{n_{conv}}+([PTH]_p)^{n_{conv}}}$. CaSR in the proximal tubule of the kidney inhibits production of $1,25(OH)_2D_3$, which is represented by $f_{CaSR-act} = \frac{1}{1+\gamma_{conv}^{Ca}[Ca^{2+}]_p}$. $1,25(OH)_2D_3$ has a self-inhibitory effect on its own production, which is represented by $f_{1,25(OH)_2D_3-act} = \frac{1}{1+\gamma_{conv}^{1,25(OH)_2D_3}[1,25(OH)_2D_3]_p}$. The regulation of $1,25(OH)_2D_3$ production by Mg^{2+} is represented by the following equation[23]:

$$f_{Mg-act} = h_m \times f_{Mg-act}^1 + (1 - h_m) \times f_{Mg-act}^2 \quad \text{(Equation 8)}$$

where h_m controls the weightage given to each function and depends on the plasma Mg^{2+} concentration and is defined as $h_m = \frac{1}{1+\left(\frac{[Mg^{2+}]_p}{[Mg^{2+}]_{thres-1,25(OH)_2D_3}}\right)^{50}}$. The parameter $[Mg^{2+}]_{thres-1,25(OH)_2D_3}$ = 2.4 mM. The terms f^1_{Mg-act} and f^2_{Mg-act} are defined as

$$f^1_{Mg-act} = \delta_{Mg-act} \times \frac{\left([Mg^{2+}]_p\right)^4}{\left(K^1_{Mg-act}\right)^4 + \left([Mg^{2+}]_p\right)^4} \quad \text{(Equation 9)}$$

$$f^2_{Mg-act} = \delta_{Mg-act} \times \frac{\left(K^2_{Mg-act}\right)^4}{\left(K^2_{Mg-act}\right)^4 + \left([Mg^{2+}]_p\right)^4} \quad \text{(Equation 10)}$$

The parameters δ_{Mg-act}, K^1_{Mg-act}, and K^2_{Mg-act} were estimated by fitting to experimental data reported in ref.[23] The comparison between model results and experimental data is given in Figure 3.

The degradation of $1,25(OH)_2D_3$ is mediated by 24-hydroxylase. PTH has a negative effect on this enzyme, whereas Mg^{2+} has a positive effect (Figure 10). The effect of PTH is represented by $f_{PTH-inact} = \frac{1}{1+\gamma^{PTH}_{inact}[PTH]_p}$ and the effect of Mg^{2+} is represented by $f_{Mg-inact} = \frac{([Mg^{2+}]_p)^4}{(K_{D3})^4+([Mg^{2+}]_p)^4}$. Model parameters are given in Table 2.

Proximal tubule of the kidney

About 15-20% of the filtered Mg^{2+} is reabsorbed paracellularly along the proximal tubule. PTH indirectly inhibits Mg^{2+} reabsorption in the proximal tubule by inhibiting the activity of NHE3. Since Na^+ reabsorption is accompanied by water reabsorption, less water is reabsorbed which reduces the lumen-to-interstitium Mg^{2+} concentration gradient; this results in decreased paracellular reabsorption of Mg^{2+}. We model the fractional reabsorption of Mg^{2+} in the proximal tubule as:

$$\lambda_{Mg-PT} = \lambda^0_{Mg-PT} + \frac{\delta^{max}_{Mg-PT}}{1+\left(\frac{[PTH]_p}{PTH_{ref}}\right)^{n_{PT}}}. \quad \text{(Equation 11)}$$

λ^0_{Mg-PT}, which denotes the minimal fractional reabsorption of Mg^{2+} in the proximal tubule, is assumed to be 0.185 and δ^{max}_{Mg-PT}, which denotes the maximal stimulation of Mg^{2+} reabsorption in the proximal tubule by PTH, is assumed to be 0.015. These parameters yield a maximum value of λ_{Mg-PT} of 0.20.

Thick ascending limb of the kidney

Along the cortical thick ascending limb, about 60-70% of the filtered Mg^{2+} is reabsorbed, again via the paracellular pathway. In this segment Mg^{2+} reabsorption is upregulated by PTH and downregulated by CaSR through claudin 14 [85]. Claudin 14 inhibits claudins 16 and 19, which regulate paracellular permeability of Ca^{2+} and Mg^{2+} along the thick ascending limb. Activation of PTH1R (PTH receptor on the basolateral membrane) decreases claudin 14 expression, whereas activation of CaSR increases claudin 14 expression.[85] The fractional reabsorption of Mg^{2+} along the thick ascending limb is modelled as

$$\lambda_{Mg-TAL} = \lambda^0_{Mg-TAL} + \delta_{TAL,CASR}\left([Ca^{2+}]_p, [Mg^{2+}]_p\right) + \delta_{TAL,PTH}(PTH) \quad \text{(Equation 12)}$$

where

$$\delta_{TAL,CASR}\left([Ca^{2+}]_p, [Mg^{2+}]_p\right) = \frac{\delta^{max}_{Mg-CaSR}}{\left(1+\left(\frac{[Ca^{2+}]_p}{Ca_{ref}}\right)^{n_{TAL}}\right)\left(1+0.6\left(\frac{[Mg^{2+}]_p}{Mg_{ref}}\right)^{n_{TAL}}\right)} \quad \text{(Equation 13)}$$

and

$$\delta_{TAL,PTH}(PTH) = \frac{\delta^{max}_{Mg-PTH}[PTH]_p}{[PTH]_p + K^{PTH}_{TAL}}. \quad \text{(Equation 14)}$$

λ^0_{Mg-TAL} denotes the minimal fractional reabsorption of Mg^{2+} in this segment and is set to be 0.66.; $\delta^{max}_{Mg-CaSR}$, which denotes the maximal stimulation of Mg^{2+} reabsorption by CaSR, is taken to be 0.028; and δ^{max}_{Mg-PTH}, which denotes the maximal stimulation of Mg^{2+} reabsorption by PTH, is set to be 0.012. Together these parameters yield a maximum value of λ_{Mg-TAL} of 0.7.

Distal convoluted tubule of the kidney

Mg^{2+} is reabsorbed transcellularly along the distal convoluted tubule mediated by TRPM6/7 on the apical membrane and Na-Mg exchanger (solute carrier family 41 member 1 (SLC41A1) and/or cyclin M2 (CNNM2)) on the basolateral membrane, with a fractional reabsorption rate of 5-10%. In this segment, Mg^{2+} reabsorption is upregulated by PTH and $1,25(OH)_2D_3$. PTH regulates Mg^{2+} uptake through receptor-mediated cAMP release and activation of protein kinase A and $1,25(OH)_2D_3$ regulates Mg^{2+} uptake through calbindin-D.[86] We assume that the contribution of PTH is greater than that of $1,25(OH)_2D_3$.[3]

$$\lambda_{Mg-DCT} = \lambda^{0}_{Mg-DCT} + \delta_{DCT}(PTH, D_3) \quad \text{(Equation 15)}$$

where

$$\delta_{DCT}(PTH, D_3) = \delta^{max}_{Mg-DCT}\left(0.8 \times \frac{[PTH]_p}{[PTH]_p + K^{PTH}_{DCT}} + 0.2 \times \frac{\left[1,25(OH)_2D_3\right]_p}{\left[1,25(OH)_2D_3\right]_p + K^{1,25(OH)_2D_3}_{DCT}}\right) \quad \text{(Equation 16)}$$

λ^{0}_{Mg-DCT}, which denotes the minimal fractional reabsorption of Mg^{2+} in this segment, is assumed to be 0.08 and δ^{max}_{Mg-DCT}, which denotes the maximal stimulation of Mg^{2+} reabsorption by PTH and $1,25(OH)_2D_3$, as 0.02. Thus, the maximum value of λ_{Mg-DCT} is 0.10.

Finally, the total renal reabsorption of Mg^{2+} is defined as

$$\lambda_{Mg-reab} = \lambda_{Mg-PT} + \lambda_{Mg-TAL} + \lambda_{Mg-DCT}. \quad \text{(Equation 17)}$$

The urinary excretion of Mg^{2+} is defined as

$$\lambda_{Mg-urine} = \Phi_{GFR} \times \left[Mg^{2+}\right]_p \times \left(1 - \lambda_{Mg-reab}\right) \quad \text{(Equation 18)}$$

where Φ_{GFR} denotes the glomerular filtration rate (GFR).

Model parameters are given in Table 2. The fractional reabsorption of Ca^{2+} along the proximal tubule, thick ascending limb, and distal convoluted tubule is modeled similar to ref.[3]

Intestine

Up to 70% of dietary Mg^{2+} is absorbed in the colon. Intestinal Mg^{2+} absorption has a biphasic, non-linear relationship with luminal Mg^{2+} concentration. Studies suggest that there are at least two intestinal transport systems for Mg^{2+}: one dependent on $1,25(OH)_2D_3$ and the other independent of $1,25(OH)_2D_3$.[18,87]

Mg^{2+} absorption by the intestine consists of a non-saturable paracellular component and a saturable transcellular component.[18,87] Paracellular Mg^{2+} absorption is responsible for 11% of intestinal Mg^{2+} uptake.[18] Thus, the equation for fractional absorption of Mg^{2+} along the intestine is formulated as follows. The intestine can absorb at most 70% of the ingested Mg^{2+}. We assume that 12% of the ingested Mg^{2+} is absorbed through $1,25(OH)_2D_3$ regulation, 11% is absorbed paracellularly, and the rest (47%) is absorbed transcellularly. Thus, fractional absorption of Mg^{2+} along the intestine is given by

$$\lambda_{Mg-intestine} = I_{Mg}\left(0.11 + 0.47 \times \frac{V_{active}}{K_{active} + I_{Mg}} + 0.12 \times f^{intestine}_{1,25(OH)_2D_3}\right) \quad \text{(Equation 19)}$$

where $f^{intestine}_{1,25(OH)_2D_3} = \frac{\left(\left[1,25(OH)_2D_3\right]_p\right)^2}{\left(\left[1,25(OH)_2D_3\right]_p\right)^2 + \left(K^{1,25(OH)_2D_3}_{abs}\right)^2}$ represents the stimulation of Mg^{2+} by $1,25(OH)_2D_3$. I_{Mg} denotes dietary Mg^{2+} intake, V_{active} denotes the maximal rate of active absorption of Mg^{2+}, K_{active} denotes the stimulation of active Mg^{2+} absorption by dietary Mg^{2+} intake, and $K^{1,25(OH)_2D_3}_{abs}$ denotes the stimulation of Mg^{2+} absorption by $1,25(OH)_2D_3$.

Bones

Of the total body magnesium, about 50–60% is found in the bones where it accounts for about 1% of bone ash.[19,88] One third of the bone Mg^{2+} is surface limited and easily exchangeable with plasma (referred to as the fast bone pool) for maintaining a normal extracellular Mg^{2+} concentration.[19,88] The remainder is complexed with the crystalline structure of bone mineral within the hydroxyapatite lattice (referred to as the slow bone pool), which may be released during bone resorption.

The change in the amount of Mg^{2+} in the readily exchangeable fast bone pool (N_{Mg_f}) is defined as

$$\frac{dN_{Mg_f}}{dt} = k^{Mg}_{p-f}\left[Mg^{2+}\right]_p V_p - k^{Mg}_{f-p} N_{Mg_f} - \tau_{ac} N_{Mg_f} \quad \text{(Equation 20)}$$

where k^{Mg}_{p-f} denotes the rate of Mg^{2+} uptake from the plasma by the fast bone pool, k^{Mg}_{f-p} denotes the rate of Mg^{2+} release from the fast bone pool to the plasma, and τ_{ac} denotes the rate of accretion into the slow bone pool.

The amount of Mg^{2+} in the slow bone pool (N_{Mg_s}) varies with time as

$$\frac{dN_{Mg_s}}{dt} = \gamma_{ac}^{Mg} N_{Mg_f} - \tau_{res}\left(PTH, 1, 25(OH)_2D_3\right). \quad \text{(Equation 21)}$$

Bone resorption rate ($\tau_{res}(PTH, 1, 25(OH)_2D_3)$) is given by[3]

$$\tau_{res}\left(PTH, 1, 25(OH)_2D_3\right) = \tau_{res}^{min} + \delta_{res}^{max}\left(0.2 \times f_{PTH}^{res} + 0.8 \times f_{1,25(OH)_2D_3}^{res}\right) \quad \text{(Equation 22)}$$

where $f_{PTH}^{res} = \frac{([PTH]_p)^2}{(K_{res}^{PTHp})^2 + ([PTH]_p)^2}$ represents the effect of PTH on bone resorption, and $f_{1,25(OH)_2D_3}^{res} = \frac{([1,25(OH)_2D_3]_p)^2}{(K_{res}^{1,25(OH)_2D_3})^2 + ([1,25(OH)_2D_3]_p)^2}$ represents the effect of $1,25(OH)_2D_3$ on bone resorption. PTH indirectly stimulates osteoclasts (bone cells responsible for resorption) by binding to receptors on osteoblasts (bone-forming cells), which then release receptor activator of nuclear factor kappa-B ligand (RANKL) and osteoprotegerin (OPG) that stimulate osteoclast formation and activity.[89] In addition, $1,25(OH)_2D_3$ enhances bone resorption by promoting the differentiation of osteoclast precursors into mature osteoclasts by increasing the expression of RANKL.[90]

Plasma magnesium

The rate of change of plasma Mg^{2+} concentration is modeled by

$$\frac{d\left[Mg^{2+}\right]_p}{dt} = \frac{\left(1 - \kappa_{b-Mg}\right)}{V_p}\left(\lambda_{Mg-intestine} + \tau_{res}\left(PTH, 1, 25(OH)_2D_3\right) + k_{f-p}^{Mg} N_{Mg_f} - k_{p-f}^{Mg}\left[Mg^{2+}\right]_p - \lambda_{Mg-urine}\right) \quad \text{(Equation 23)}$$

where κ_{b-Mg} denotes the fraction of magnesium bound to proteins. All model parameters and descriptions are given in Table 2.

QUANTIFICATION AND STATISTICAL ANALYSIS

The model was implemented in MATLAB. The **lsqcurvefit** function of MATLAB, which is a non-linear least-square solver, was used to fit our model simulations to experimental values and this is mentioned in the legends of Figures 2 and 3.